

# BMC Systems Biology

## Pathobiochemical signatures of cholestatic liver disease in bile duct ligated mice

--Manuscript Draft--

<b>Manuscript Number:</b>	
<b>Full Title:</b>	Pathobiochemical signatures of cholestatic liver disease in bile duct ligated mice
<b>Article Type:</b>	Research article
<b>Section/Category:</b>	Systems physiology, pharmacology and medicine
<b>Abstract:</b>	<p><b>Background:</b> Disrupted bile secretion leads to liver damage characterized by inflammation, fibrosis, eventually cirrhosis, hepatocellular cancer, loss of organ function and death. As obstructive cholestasis often progresses insidiously, early diagnosis and an adequate therapy are urgently needed. To better understand the cascade of histological and biochemical alterations, a comprehensive data set of serum markers, histological parameters and transcript profiles was compiled at 8 time points after bile duct ligation in mice, comprising different stages of the disease.</p> <p><b>Results:</b> A thorough statistical analysis of these 6,313 data points revealed distinct temporal phases of disease development and progression, on account of histological presentation and pattern of molecular changes. Histological count of CTGF-positive cells provided the most reliable overall measure for disease progression, closely correlated to TGF-<math>\beta</math> expression. Onset of disease is marked best by fibronectin, transition to the perpetuation phase by interleukin 2, and the progression phase by interleukin 28-<math>\beta</math>. Prominent molecular events exhibited by strong transcript peaks are found for small heterodimer partner at 6 h and transin-2 at 18 h. Predictive decision trees for disease phases suggest the existence of well-coordinated and individually reproducible pathobiochemical signatures.</p> <p><b>Conclusion:</b> These results are the basis to discover the relevant molecular interactions and suggest novel markers of the disease process that can be used for diagnosis and therapy.</p>
<b>Corresponding Author:</b>	Kerstin Abshagen Institute for Experimental Surgery Rostock, GERMANY
<b>Corresponding Author Secondary Information:</b>	
<b>Corresponding Author's Institution:</b>	Institute for Experimental Surgery
<b>Corresponding Author's Secondary Institution:</b>	
<b>First Author:</b>	Kerstin Abshagen
<b>First Author Secondary Information:</b>	
<b>Order of Authors:</b>	Kerstin Abshagen Andreas Hoppe Maria Thomas Isabell Müller Matthias Ebert Honglei Weng Herrmann-Georg Holzhütter Ulrich M Zanger Johannes Bode Brigitte Vollmar Steven Dooley
<b>Order of Authors Secondary Information:</b>	

1 Abshagen et al. Cellular and molecular signatures of cholestasis

2

3

4

5

6

**Pathobiochemical signatures of cholestatic liver disease****in bile duct ligated mice**

10

11

12

13

14

15

16

17

18

19

20

21

22

23

24

25

26

27

28

29

30

31

32

33

34

35

36

37

38

39

40

41

42

43

44

45

46

47

48

49

50

51

52

53

54

55

56

57

58

59

60

61

62

63

64

65

**Kerstin Abshagen<sup>1†\*</sup>, Andreas Hoppe<sup>2†</sup>, Maria Thomas<sup>3</sup>, Isabell Müller<sup>1</sup>, Matthias Ebert<sup>4</sup>, Honglei Weng<sup>4</sup>, Herrmann-Georg Holzhütter<sup>2</sup>, Ulrich M. Zanger<sup>3</sup>, Johannes Bode<sup>5</sup>, Brigitte Vollmar<sup>1</sup>, Steven Dooley<sup>4</sup>**<sup>1</sup>Institute for Experimental Surgery, University Medicine Rostock, 18057 Rostock, Germany<sup>2</sup>Institute for Biochemistry, Computational Systems Biochemistry Group, Charité University Medicine Berlin, 10117 Berlin, Germany<sup>3</sup>Dr. Margarete Fischer-Bosch Institute of Clinical Pharmacology, 70376 Stuttgart, and University of Tuebingen, Tuebingen, Germany<sup>4</sup>Department of Medicine II, Section Molecular Hepatology, Medical Faculty Mannheim, Heidelberg University, 68167 Mannheim, Germany<sup>5</sup>Department for Gastroenterology, Hepatology and Infectiology, Heinrich-Heine University of Düsseldorf, 40225 Düsseldorf

\*These authors contributed equally to this work

Correspondence should be addressed to:

Kerstin Abshagen, PhD

Institute for Experimental Surgery

Rostock University Medical Center

Schillingallee 69a

18057 Rostock

Germany

phone: +49 381 494 2503

fax: +49 381 494 2502

E-mail: [kerstin.abshagen@uni-rostock.de](mailto:kerstin.abshagen@uni-rostock.de)

4   **1 Email addresses:**

5    2 andreas.hoppe@charite.de  
6

7    3 Maria.Thomas@ikp-stuttgart.de  
8

9    4 isabell-mueller86@web.de  
10

11    5 matthias.ebert@umm.de  
12

13    6 honglei.weng@medma.uni-heidelberg.de  
14

15    7 hergo@charite.de  
16

17    8 Uli.Zanger@ikp-stuttgart.de  
18

19    9 Johannes.Bode@med.uni-duesseldorf.de  
20

21    10 brigitte.vollmar@med.uni-rostock.de  
22

23    11 Steven.Dooley@medma.uni-heidelberg.de  
24

25    12  
26

27    13 **Running title:** Cellular and molecular signatures of cholestasis  
28

29    14  
30

31    15  
32

33    16  
34

35    17  
36

37

38

39

40

41

42

43

44

45

46

47

48

49

50

51

52

53

54

55

56

57

58

59

60

61

62

63

64

65

3

4

## 5 Abstract

6

7

8

9

10

11

12

13

14

15

16

17

18

19

20

21

22

23

24

25

26

27

28

29

30

31

32

33

34

35

36

37

38

39

40

41

42

43

44

45

46

47

48

49

50

51

52

53

54

55

56

57

58

59

60

61

62

63

64

65

2 **Background:** Disrupted bile secretion leads to liver damage characterized by inflammation, fibrosis,  
3 eventually cirrhosis, hepatocellular cancer, loss of organ function and death. As obstructive cholestasis  
4 often progresses insidiously, early diagnosis and an adequate therapy are urgently needed. To better  
5 understand the cascade of histological and biochemical alterations, a comprehensive data set of serum  
6 markers, histological parameters and transcript profiles was compiled at 8 time points after bile duct  
7 ligation in mice, comprising different stages of the disease. **Results:** A thorough statistical analysis of  
8 these 6,313 data points revealed distinct temporal phases of disease development and progression, on  
9 account of histological presentation and pattern of molecular changes. Histological count of CTGF-positive  
10 cells provided the most reliable overall measure for disease progression, closely correlated to TGF- $\beta$   
11 expression. Onset of disease is marked best by fibronectin, transition to the perpetuation phase by  
12 interleukin 2, and the progression phase by interleukin 28- $\beta$ . Prominent molecular events exhibited by  
13 strong transcript peaks are found for small heterodimer partner at 6 h and transin-2 at 18 h. **Predictive**  
14 decision trees for disease phases suggest the existence of well-coordinated and individually reproducible  
15 pathobiochemical signatures. **Conclusion:** These results are the basis to discover the relevant molecular  
16 interactions and suggest novel markers of the disease process that can be used for diagnosis and  
17 therapy.

18  
19 **Keywords:** liver injury, mouse, systems biology, fibrosis, cell proliferation, bile duct ligation, cholestasis,  
20 morphological profiling, VirtualLiver Network

3  
4 **1 Background**

5  
6 Development and progression of chronic liver diseases (CLD) is a highly dynamic process that  
7 comprises a complex cytokine mediated communication network of the different liver cell types that results  
8 in cellular plasticity with impact on organ function (see Figure 1 in [1]). The cascade is initiated in all  
9 entities of liver diseases by hepatocyte damage with subsequent necrosis and apoptosis (probably also  
10 necroptosis). Factors from dying hepatocytes are flooding the neighborhood, get in contact with the  
11 surface of surrounding cells and initiate a wound healing response, comprising, among others, activation  
12 of hepatic stellate cells (HSC) and Kupffer cells (KC, the liver resident macrophages). Activated HSC and  
13 KC change their original phenotype, and by active secretion of a multiplicity of factors, become the drivers  
14 of subsequent steps of the cascade, that is recruitment of inflammatory cell populations and formation of a  
15 wound closing extracellular matrix. If the insult occurs as an acute event, subsequent regenerative  
16 processes are dominant and liver homeostasis is reached very fast [2]. However, insulting the liver, e.g. by  
17 alcohol, virus infection or drug medication, are usually continuous events resulting in a chronic cycle of  
18 damage and repair. This frequently leads to disease progression with inflammation, fibrosis (scarring),  
19 cirrhosis, hepatocellular cancer and finally loss of organ function and death. Patients generally present in  
20 the clinic with already advanced disease stages. Therefore, there is urgent need for improved diagnostics  
21 and antifibrotic therapies to prevent progression toward cirrhosis [3].

22 In the quest for new antifibrotic therapies, the mechanisms behind the above described complex  
23 multicellular network are the basis for a new generation of clinical strategies - the combination of high  
24 throughput diagnostics and individualized therapy. Currently, translational research is still vertical  
25 movement of knowledge from bench to bedside with restriction to a few selected disease-related  
26 molecular processes. Pharmaceutical therapies focusing on a single or a few targets represent an  
unpredictable perturbation of the complex biological network and thus, bear the risk of inefficacy and  
severe unwanted side effects. Moreover, in different phases of a CLD, the relative importance of distinct  
molecular processes as, for example, up-regulation of pro-inflammatory cytokines or pro-fibrotic metabolic  
enzymes, changes considerably. The translational goal - identification of critical process knot points -

4     1 requires mathematical modeling that may take into account multiple parallel processes, process dynamics,  
5     2 and experimental data from different levels of cellular organization [4].  
6

7         3 In recent years, we have gained tremendous insight into molecular and cellular mechanisms of CLD  
8         4 progression of all the different etiologies. Yet, given the vast complexity of the molecular processes  
9         5 involved, this knowledge is still fragmented and we are far from a comprehensive and predictive  
10        6 mathematical model that could be used in a clinical context. Molecular mechanisms identified from basic  
11        7 research and disease stage specific phenomenological observations need to be integrated into a holistic  
12        8 framework characterized by concurrent parallel processes, which is the main objective of the presented  
13        9 work.  
14

15         10 A CLD in a patient represents with characteristic morphologic, biochemical and molecular changes in  
16        11 liver and blood that can be scored qualitatively and quantitatively, and the assessments can be combined  
17        12 to stratify different CLD patients into subgroups, e.g. showing common features regarding disease  
18        13 progression and survival. Semiquantitative morphological scoring is still the standard technique for  
19        14 histologic grading in CLD. More recently, considerable effort has been devoted to high throughput  
20        15 molecular profiling for diagnosis and assessment of disease progression. However, handling huge  
21        16 amounts (high content) of such data to draw robust conclusions for clinical translation is still in its  
22        17 beginnings. Therefore, the aim of our study was to correlate high-accuracy image data and transcriptional  
23        18 profiles of a number of preselected targets with pathobiochemistry data, all obtained at different time  
24        19 points after onset of obstructive cholestasis, to identify the most significant and unambiguous molecular  
25        20 markers for different phases of disease development. With that, we expected to receive several biological  
26        21 hits that would provide new insight into mechanisms driving disease progression.  
27

28         22 As an example, we have used BDL in mice [5], a classic experimental model for secondary biliary  
29        23 fibrosis. BDL pathophysiology comprises proliferation of biliary epithelial cells (BECs), oval cells and  
30        24 HSCs, resulting in proliferating bile ductules, cholestasis, portal inflammation and fibrosis, causing  
31        25 secondary biliary cirrhosis, ultimately leading to liver failure. From 8 different time points of disease  
32        26 progression, we have collected more than 6,000 experimental data points, comprising  
33        27 immunohistochemistry, biochemistry and molecular profiling measures.  
34

4 Statistical methods have been applied to unravel robust interrelations in this complex data set. We  
5 correlated level and timing of pathophysiological events with transcriptional changes in order to define  
6 molecular markers, and developed decision trees that allow assessment of the different disease phases  
7 occurring during the development of cholestasis.

8  
9  
10  
11  
12  
13 **Materials and Methods**

14  
15 **Ethic Statement**

16 All experiments were approved by the local government Landesamt für Landwirtschaft,  
17 Lebensmittelsicherheit und Fischerei Mecklenburg-Vorpommern (LALLF M-V/TSD/7221.3-1.2-049/09) and  
18 performed in accordance with the German legislation on protection of animals and the National Institutes  
19 of "Health Guide for the Care and Use of Laboratory Animals" (Institute of Laboratory Animal Resources,  
20 National Research Council; NIH publication 86-23 revised 1985).

21  
22 **Mice**

23 Male C57BL/6J (Charles River Laboratories, Sulzfeld, Germany) at 8–10 weeks of age with a body  
24 weight of 23–26 g were kept on water and standard laboratory chow ad libitum.

25  
26 **Surgical procedure and experimental groups**

27 Mice were anesthetized by breathing isoflurane (1.5 vol%). BDL was performed after midline  
28 laparotomy. The common bile duct was ligated three times with 5-0 silk and transected between the two  
29 most distal ligations. Sham operation was performed similarly, except for ligation and transection of the  
30 bile duct (0 h, n=5). All surgical procedures were performed under aseptic conditions. Animals were  
31 allowed to recover from anesthesia and surgery under a red warming lamp and were held in single cages  
32 until subsequent experiments followed at postoperative hours 6, 12, 18 and 30 (n=5 animals per time  
33 point), and at 2, 5 and 14 days after BDL (n=5 animals per time point). Sham-operated animals without  
34 BDL served as controls (n=5). To analyze the regenerative response in regard to proliferation of different  
35 cell types, 5-bromo-2-deoxyuridine (BrdU; 50 mg/kg bw ip) was injected 1 h prior to harvest of liver tissue.  
36 BrdU incorporation into DNA was analysed by immunohistochemistry. To obtain blood and liver samples,  
37 mice were killed at the indicated time points. Liver tissue was partially embedded in paraffin for  
38 morphology analysis and snap frozen for molecular biology and biochemistry analyses. In addition, liver  
39

4 1 tissue served for the parallel Taqman qRT-PCR using microfluidic Fluidigm Biomark™ platform (Fluidigm,  
5  
6 CA, USA).

7  
8     **Hematological measurements and plasma enzyme levels**

9  
10 4 Animals were anesthetized and exsanguinated by puncture of the vena cava inferior. Red blood cell  
11  
12 5 and blood platelets count, hemoglobin, and hematocrit were assessed with an automated cell counter  
13  
14 6 (Sysmex KX-21, Sysmex). Plasma activities of alanine aminotransferase (ALT), aspartate  
15  
16 7 aminotransferase (AST) and glutamate dehydro-genase (GLDH) were measured spectrophotometrically.

17  
18     **Assays**

19  
20 9 EDTA plasma served for the analysis of albumin as a parameter of liver function, which was  
21  
22 10 determined with a commercially available enzyme-linked immunosorbent assay kit in accordance with the  
23  
24 11 manufacturer's instructions (Assaypro, MO, USA).

25  
26     **Histopathology and image analysis**

27  
28 13 Liver tissue samples were fixed in formalin for 2 to 3 days and embedded in paraffin. 5 µm sections  
29  
30 14 were stained with hematoxylin and eosin (H&E) for routine examination and quantification of bile infarcts.  
31  
32 15 Sirius red staining served for quantification of collagen deposition. All samples from a series of  
33  
34 16 experiments were stained simultaneously and evaluated in a blinded manner. For histomorphometric  
35  
36 17 analysis, images of 20 random low power fields (x10 magnification, Olympus BX 51, Hamburg, Germany)  
37  
38 18 were acquired with a Color View II FW camera (Color View, Munich, Germany) and evaluated using an  
39  
40 19 image analysis system (Adobe Photoshop, Adobe Systems, Uxbridge, UK). Fibrosis deposition was  
41  
42 20 quantified as a percentage of Sirius red stained area compared with the total section area. The surfaces of  
43  
44 21 large centrilobular veins and large portal tracts were excluded from this calculation. Bile infarcts were  
45  
46 22 quantified in H&E-stained sections in a similar manner and the percentage of the focal necrosis surface to  
47  
48 23 the whole liver section area was assessed.

49  
50     **Immunohistochemistry and image analysis**

51  
52 25 For analyzing DNA-incorporated BrdU in liver cells, 4 µm sections collected on poly-L-lysine-coated  
53  
54 26 glass slides were incubated with monoclonal mouse anti-BrdU antibody (1:50; Dako Cytomation,  
55  
56 27 Hamburg, Germany) overnight at 4°C, followed by horseradish-peroxidase (HRP)-conjugated goat anti-  
57  
58 28 mouse immunoglobulin (LSAB kit plus; Dako). Sites of peroxidase-binding were detected by 3,3'-

4 1 diaminobenzidine (Dako). Sections were counterstained with hemalaun. BrdU-positive hepatocellular  
5 2 nuclei were counted in a blinded manner within 30 consecutive high power fields (HPF) (x40 objective,  
6 3 numerical aperture 0.65) and are given as cells/mm<sup>2</sup>. In analogy, BrdU-expressing non-parenchymal cells  
7 4 were assessed and also given as cells/mm<sup>2</sup>.

8 To specify the proliferative response of non-parenchymal cells upon BDL, we performed double  
9 immunohistochemistry of BrdU with specific markers for different liver cells: F4-80/BrdU for Kupffer cells  
10 and SM22α/BrdU for BEC. For each protocol, the immune-staining procedure for the specific marker was  
11 conducted after the BrdU staining protocol. Resident liver macrophages were analyzed using the F4-80  
12 antigen (1:10; Serotec, Oxford, UK). Overnight incubation (4°C) with the first antibody (polyclonal rat anti-  
13 F4-80) was followed by alkaline-phosphatase (AP) conjugated mouse anti-rat immunoglobulin (1:200;  
14 Santa Cruz Biotechnology, Santa Cruz, CA, USA). The sites of AP-binding were detected using the  
15 chromogen fuchsin (Dako).

16 BECs and oval cells were detected by overnight incubation (4°C) with a polyclonal rabbit anti-SM22α  
17 antibody (1:100; Abcam, Cambridge, UK) followed by AP conjugated goat anti-rabbit immunoglobulin as  
18 secondary antibody (1:100; Dako). The sites of AP-binding were detected by Permanent Red (Dako).

19 Slides were viewed under a light microscope (Olympus BX 51) and the number of BrdU-positive cells  
20 co-expressing F4-80 or SM22α were counted in a blinded manner within 30 consecutive high power fields  
21 (HPF) (x40 objective, numerical aperture 0.65) and are given as cells/mm<sup>2</sup>.

22 Antibodies for detection of α-SMA in HSCs and of S100a4-positive cells were from DAKO (M0851  
23 and A5114, 1:500 and 1:200 dilution, respectively). CTGF antibody was from Santa Cruz (sc-1439, 1:200  
24 dilution). Sections were de-paraffinized in serial ethanol dilutions. After a PBS wash, sections were  
25 transferred into 10 mM sodium citrate buffer (pH 6.0) and antigen unmasking was performed in a  
26 microwave. After cooling down, sections were incubated in peroxidase blocking reagent (Dako) for 1 h and  
27 with primary antibodies overnight at 4°C. EnVision peroxidase (Dako) was applied for 1 h at room  
28 temperature after a PBS wash next day. Sections were developed with diaminobenzidine for 5 minutes.  
29 The number of α-SMA-, CTGF- and S100a4-positive cells was quantified under a Leica light microscope  
30 (x20) by counting three fields.

31 28 **High-throughput quantitative Taqman RT-PCR analysis**

4 Total RNA was isolated from the liver tissue samples using RNeasy Mini Kit including on column  
5 genomic DNA digestion with RNase free DNase Set (Qiagen, Hilden, Germany). RNA was reverse  
6 transcribed to cDNA with TaqMan Reverse Transcription Reagents (Applera GmbH, Darmstadt,  
7 Germany). For quantitative real-time PCR, we used the **Fluidigm's Biomark high-throughput qPCR chip**  
8 **platform** (Fluidigm Corporation, San Francisco, CA, USA) with pre-designed gene expression assays from  
9 Applied Biosystems, according to the manufacturer's instructions [6]. Data were analyzed using the ddCt  
10 method and expression values were normalized to the expression levels of the GAPDH gene.

11  
12     **Correlation analysis**  
13  
14

15     For each pair of factors, Pearson correlations of the average factor values were calculated for each  
16 time point (denoted Av). As this correlation ignores the variability among the mice of the same time point,  
17 also Pearson correlations for all measurements were calculated (denoted All). As factor correlations may  
18 differ for specific time ranges, they were also computed for the mice of each single time point (denoted  
19 T0h ... T14d) and for all time ranges of 2 and 3 consecutive time points (denoted 6-18h ... 2-5d). This set  
20 of 21 correlations was combined to a single "consensus correlation" as a weighted sum of the positive part  
21 of the correlation weighted by a significance-dependent factor, the p-value of the associated t-test.  
22 Significance was estimated with a two-sample t-test for the likelihood of correlation, and is displayed as  
23 shades of yellow in Figs. 7 and 8. Similarly, a consensus correlation is computed for the negative parts,  
24 representing anti-correlation. The final consensus score is the larger of both, displayed as shades of green  
25 in Figs. 7 and 8. See Supporting Information dataset S2 for details.

26     Hierarchical clustering was performed based on the consensus correlations, choosing Weighted Pair-  
27 Group Method for the distance of clusters. The computations have been performed with **R** ([www.r-project.org](http://www.r-project.org)). The circular dendrogram shown in Figure 7 has been drawn using ape package (ape-  
28 package.ird.fr) using colors generated with Sciences-Po Medialab tools (tools.medialab.sciences-  
29 po.fr/iwanthue).

30  
31     **Predictions of time point/phase of disease development**  
32  
33

34     First, the factors were analyzed for their suitability to predict a time frame on its own. Here, a time  
35 frame is defined by a start and end time point, such as 6-18h or 0h-14d. Iteratively through all time points  
36 and possible time frames, it is checked whether the values of a given variable in and out of the time frame  
37  
38  
39  
40  
41  
42  
43  
44  
45  
46  
47  
48  
49  
50  
51  
52  
53  
54  
55  
56  
57  
58  
59  
60  
61  
62  
63  
64  
65

1 have disjoint value ranges, in which case it is called separator. A separator is evaluated by the gap  
2 between both value ranges in relation to the total value range, e.g. if the values of the time points 0h-30h  
3 lie between 0 and 2 and for the range 2d-14d between 3 and 10, the relative gap is  $0.1 = (3-2)/(10-0)$ .

5 For the automatic generation of decision trees, separators for smaller time frames are used. For  
6 instance, after the 0h-14d has been split into 0h-2d and 5d-14d, to separate 0h-2d further, the values of  
7 5d and 14d are ignored, allowing more separators. Again, these separations are quantified by the relative  
8 gap of the separation. To compute a decision tree, the time range 0h-14d is recursively separated by the  
9 best available separator for the respective time frame.

11 This procedure was applied to the data of all mice to generate the decision trees. For testing the  
12 predictive capacity of the automatically generated decision trees, the data for one mouse was left out, the  
13 decision tree was computed again, and the omitted mouse was then categorized using the decision tree.

15 **This process was repeated for all mice. It has to be noted that the decision trees are different for each**  
16 **iteration and the decision trees in Figure 11 recalls all data but is not tested on an unknown mouse. The**  
17 **mouse for which no transcript abundances were measured was excluded from the leave-one-out test,**  
18 **totaling 40 tests.**

20 As the histopathological parameters (e.g. CTGF-positive cells) are only measured for 3 of the 5  
21 repeats, it may happen that a computed decision tree is not applicable to a particular mouse, i.e. if a node  
22 in the decision tree quests for but this data is not measured, this case is specifically marked.

24 The same procedure is applied for the decision trees for the phases (0h, 6-12h, 18h-2d, and 5-14d)  
25 instead of individual time points.

## 27 Statistical analysis

29 All data are expressed as means  $\pm$  SEM. To assess whether a parameter changes in the time course,  
30 a one-way ANOVA test was applied. To assess whether the transition from one time point to another is  
31 significantly changes, a two-sample t-test was applied. For each parameter pair, a 2-MANOVA was  
32 performed, and tested with Pillai, Wilks, Hotelling-Lawley, and Roy test. The significance figure was  
33 ranked for each test, and a combined ranking is computed. Then, for each parameter pair a linear  
34 discriminant analysis was performed. It is tested with a leave-one-out cross-validation. The list of  
35 parameter pairs is sorted by the ratio of correct predictions. The calculations have been performed in R,  
36 37 38 39 40 41 42 43 44 45 46 47 48 49 50 51 52 53 54 55 56 57 58 59 60 61 62 63 64 65

4 1 using the functions t.test, aov, and lda. Normality tests were performed with the Shapiro-Wilk test,  
5 2 implemented in the R package nortest. For 85% of factor/time point combinations, normal distribution was  
6 3 not excluded. See the respective sections in Supporting Information Dataset S4.  
7  
8

9  
10 4 **Results and Discussion**  
11  
12

13 5 In mice, BDL over 14 days induces time dependently progressing stages of a secondary biliary CLD.  
14 6 The first week after BDL begins with an acute cholestatic injury associated with necroinflammation,  
15 7 followed by a chronic injury stage, comprising hepatitis and liver fibrosis. Macroscopically, marked dilation  
16 8 of the gallbladder and formation of bilioma are found, associated with weight loss and a mortality rate of  
17 9 10% in the first week due to bile leakage and rupture of the gallbladder [7]. Pathophysiologically, BDL  
18 10 interferes with glandular liver function and hepatobiliary transport, which comprises its detoxification and  
19 11 secretion function including bile formation. Obstruction of the bile duct leads to afflux of newly generated  
20 12 bile fluid. The main components of the bile, bile acids and phospholipids, induce toxicity and damage  
21 13 towards hepatocytes and cholangiocytes, therewith initiating the disease process. **Rapidly after BDL, mice**  
22 14 **develop obstructive jaundice and cholestasis, as displayed by markedly elevated serum transaminases**  
23 15 **and bilirubin levels (Figure 1), macroscopically evident from yellow ears and urine.** Within the first 30 h,  
24 16 there is a massive release of liver enzymes, like ALT and GLDH, reflecting the initial hepatocyte damage  
25 17 as first pathophysiological event in the process of BDL-induced liver fibrosis (Figures 1A, B). Afterwards,  
26 18 levels of enzymes remain more or less constant throughout the time course, indicating acute cholestatic  
27 19 cell death, except the 14 days value, which interestingly decreased to levels only slightly above those of  
28 20 sham operated liver. Concomitantly, liver detoxification capacity becomes deteriorated, as displayed by  
29 21 the rise of total bilirubin, a classical plasma marker of cholestasis (Figure 1C). Interestingly, despite the  
30 22 disturbance of liver homeostasis, albumin synthesis as a global parameter of liver function is maintained  
31 23 relatively constant over the observation period of 14 d (Figure 1D). Analysis of systemic blood cell count  
32 24 reveals constant levels of erythrocytes and platelets up to day 5 (Table 1). In contrast, leukocytes  
33 25 decrease by 50% during the first 2 d, reflecting intrahepatic cell entrapment, and recover to values of  
34 26 sham operated animals within the subsequent observation period (Table 1). During progression of fibrosis,  
35 27 red blood cells, hemoglobin and hematocrit slightly decrease.  
36  
37  
38  
39  
40  
41  
42  
43  
44  
45  
46  
47  
48  
49  
50  
51  
52  
53  
54  
55  
56  
57  
58  
59  
60  
61  
62  
63  
64  
65

2  
3  
4 In consequence of intrahepatic toxic bile accumulation, progressive development of confluent bile  
5 lakes is typical, and histological quantification of bile infarcts, defined as clusters of injured hepatocytes,  
6 revealed a steady rise of infarct areas until day 14 after BDL (Figure 2A). This is exemplified in Figure 2B,  
7 which shows the typical appearance of liver tissue at representative time points after BDL using H&E  
8 staining. Further histopathological changes of the livers after BDL include enlargement of portal tracts,  
9 accompanied by dilation of bile canaliculi and proliferation of BECs and oval cells (Figure 3A), resulting in  
10 formation of artificial bile ductules (Figure 2C), a cellular response termed 'ductular reaction' [5; 8].  
11 Unexpectedly, recent data from lineage tracing experiments indicated that these cells, however, do not  
12 contribute to the population of ECM producing/fibrogenic cells, which also in the BDL model is largely  
13 consisting of HSCs [9].

14 The inflammatory response resulting from chronic hepatocyte injury comprises accumulation of  
15 immune cells in the liver, among others, T cells, macrophages and dendritic cells, mainly into and around  
16 bile infarct areas (Figure 2C, asterisk) [10]. The inflammatory and fibrogenic response is initiated by  
17 resident liver cells, e.g., Kupffer cells and activated HSCs that secrete a wide range of cytokines and  
18 chemokines and thereby influence quality and quantity of inflammatory and consequently fibrotic  
19 responses [11; 12]. Upon parenchymal damage, quiescent HSCs undergo phenotypical changes to  
20 myofibroblasts (MFBs). The most prominent role of MFBs is extracellular matrix (ECM) production and  
21 reorganization, as reflected by, among others, increased synthesis of  $\alpha$ -SMA, type I collagen and TIMPs.  
22 A marked increase of the number of  $\alpha$ -SMA- and S100a4-positive cells, as measured by  
23 immunohistochemistry, was obvious after BDL (Figures 3B, C). Migration of MFBs to the injury and their  
24 contractility contribute to liver scarring. This is accompanied by parenchymal cell proliferation, which  
25 began to rise at day 2 as regenerative response but decreased at day 14 (Figure 3D). With a slightly faster  
26 response as compared to HSCs, starting at 30 h upon BDL, Kupffer cells started to proliferate (Figure 3E).

27 The overall hepatic proliferative response as analyzed by immunohistochemistry was confirmed by  
28 elevated mRNA expression of Ki67 (Figure 4A).

29 Between 5 and 14 days after BDL, periportal alterations were associated with fibrotic changes. As  
30 demonstrated by Sirius red staining, extensive fibrosis, characterized by a several-fold increase of  
31 collagen deposition (Figure 4B), including bridging, was observed 5 days after BDL (Figure 4C). We  
32

4 further stained for connective tissue growth factor (CTGF), a prominent fibrogenic cytokine and enhancer  
5 of TGF- $\beta$  effects [13]. The number of CTGF-positive cells increased time dependent and continuously with  
6 time and severity of fibrosis, starting as early as 12 h upon BDL (Figure 3F).

7  
8  
9  
10 To investigate dynamic changes in gene expression patterns following BDL, we assessed time-  
11 resolved transcriptomics profiles of three different gene panels related to hepatocyte metabolism  
12 fibrogenesis and inflammation using the Fluidigm platform (Figure 5). The selection of representative  
13 genes for ADME- (absorption, distribution, metabolism, and excretion) (Figure 5A) fibrogenesis- (Figure  
14 5B), and inflammation-related genes (Figure 5C) was made arbitrary based on state-of the art knowledge.

15  
16 mRNA levels of genes involved in metabolism (ADME, Figure 5A), such as the classical  
17 representatives of the detoxifying cytochrom P450 system are immediately induced during the first 6 h  
18 upon damage and are then steadily decreasing with time after BDL (Figure 5A). This indicates that early  
19 after the insult, detoxification activity is increased to interfere with damage that however is too strong.  
20 Consequently, ongoing hepatocyte depletion leads to significant decreases in total liver enzyme  
21 expression and activity. Several exceptions for genes that play a role in detoxification and in antagonizing  
22 oxidative stress, such as Cyp3a11, Gsta2 or Sult1a1, exist. BDL-induced significant changes were  
23 identified for genes playing a role in the regulation of oxidative stress, e.g. Nos2 and Nfkbia.

24  
25 For example, analysis of both fibrillar collagen1 $\alpha$ 1 and 3 $\alpha$ 1, which predominantly exist in fibrotic  
26 livers, showed a significant upregulation rapidly after BDL and a continuous increase with severity of liver  
27 fibrosis up to 14 days after BDL (Figures 6E, F). Among the peptide mediators, not very surprisingly, TGF-  
28  $\beta$  (isoforms 1 and 2) mRNA expression was steadily increasing, confirming its postulated role as fibrogenic  
29 master cytokine [14]. Associated with induction of fibrogenesis-related genes (Figure 5B), which  
30 particularly are representative for HSC activation, the dynamics of the inflammation gene signature (Figure  
31 5C) nicely matches with the increase in the number of proliferating Kupffer cells (F4-80/BrdU staining  
32 values) observed from day 2 onwards (Figure 3E). Very low expression levels were present immediately  
33 after BDL, except for the chemokines Cxcl1 und 2. Starting at time points between 2 and 5 d after BDL,  
34 most cytokines and chemokines in the list were strongly upregulated for a longer period of time, until day  
35 14.

4 Taken together, the detailed time-resolved transcriptional profiling of liver homogenates following BDL  
5 revealed a coordinated induction of detoxification processes immediately after surgery and an  
6 upregulation of an inflammatory response along with activation of metabolically active genes, which can  
7 be explained by physiological recovery and adaptation of the mice to the bile acid exposure.

8  
9  
10  
11  
12 **Correlations**  
13  
14

15 To assess interrelations between level and time of pathophysiological events and predictive markers  
16 within the complex scenario of cholestatic liver disease, correlations were analyzed. The correlation of the  
17 time point averages (column Av in Figs. 7 and 8) is high for most parameter pairs, not unexpectedly, as  
18 most histologic parameters and cell count observations, as well as most genes related to inflammation  
19 and fibrogenesis increase with disease progression (about 2/3 of all factors studied). However, there is  
20 large variance in values for many analyzed factors, when comparing individual mice of the same time  
21 points. For example, at 5 days, the infarct area varies from 0.9% to 12% and the collagen deposition area  
22 varies from 0.8%-5.9%. Thus, we decided to study correlations of determined parameters from individual  
23 mice (All) with regard to time points (T0h...T14d) and time frames (6-18h and so on) to yield more specific  
24 results. With that strategy, we were able to identify, for example, parameter pairs displaying a correlation  
25 only at specific phases. As all the identified correlations, both time course and single mouse correlations,  
26 represent complementary aspects, a consensus measure is calculated, which is used for a final  
27 assessment of the relation of two factors, as shown in the hierarchical clustering in Figure 7 and to  
28 determine the ranking of correlated factors in Figs. 8 and 9.  
29  
30

31 To identify global connections between factors, the consensus correlation coefficients have been  
32 subjected to a cluster analysis (Figure 7). RNA levels of commonly regulated genes form highly correlated  
33 clusters, e.g., (i) cytokines and growth factors, such as Il6 and Tgfb (lower left, blue), (ii) fibrosis-related  
34 genes, such as Coll1a1 and Timp1 (bottom right, cyan), (iii) ADME-related genes, such as isoforms of  
35 Cyp24a1 and Nr0b2 (red, top right). There are also RNAs, which poorly correlate with any other  
36 parameter, such as Rarres1 and Igf1. GLDH as well as albumin are not well-connected with any other  
37 parameter, while serum ALT clusters with Cyp7a1 by a negative correlation. Sirius red-positive area  
38 (collagen) is quite isolated in the graph map, and most closely relates to the cytokines' cluster (left, grey).

4 1 BrdU-positive Kupffer cells, BECs and S100a4-positive cell numbers are clustered with the closely related  
5 2 RNAs of Gstm1 and Gsta2 (top left, purple, brown, light blue). BrdU-positive hepatocytes are clustered  
6 3 together with Notch1, Birc5, and Mki67 (bottom, cyan). CTGF and  $\alpha$ -SMA positive cells are clustered with  
7 4 the RNA of Pparg and Gstp1 (top left, grey blue).

8  
9  
10  
11  
12 **5 Initial response**  
13  
14

15 6 Immediately after BDL, there is a massive release of liver enzymes up to day 5, followed by a drop  
16 7 down to almost values of sham-operated livers (Figures 1A, B). It can be interpreted as the beginning  
17 8 breakdown of hepatocellular protein synthesis or the cease of cell necrosis.

18 9 The factor with the strongest negative correlation to ALT in serum is Cyp7a1 (Figure 8A). As Cyp7a1  
19 10 mRNA encodes cholesterol-7- $\alpha$ -hydroxylase, down-regulation of bile acid synthesis can be seen as a fast  
20 11 and straightforward response to cholestasis. As underlying mechanism, activation of the JNK/c-Jun  
21 12 pathway has been reported [15]. In later time phases Cyp7a1 increases again, most likely SREBP-  
22 13 mediated, since plasma cholesterol concentration increases simultaneously [16]. The second highest  
23 14 correlated factor to ALT is Hmox1, encoding heme oxygenase, which was reported as increased upon  
24 15 BDL [17]. It therefore also can be defined as “early response” parameter, which subsequently remains at  
25 16 increased levels as compared to healthy liver. GLDH is another serum marker (Figure 8B) for  
26 17 hepatocellular injury that positively correlates to ALT, but less significant than Cyp7a1 and Hmox1,  
27 18 indicating that ALT and GLDH are suitable as independent measures. Additionally, a high correlation is  
28 19 found for ALT with Cebpb, which encodes CCAAT/enhancer-binding protein  $\beta$ , a regulator of the  
29 20 inflammatory response, e.g. via up-regulating Il6 [18]. The two chemokines Cxcl1, encoding neutrophil-  
30 21 activating protein 3, and Cxcl2, encoding macrophage inflammatory protein 2- $\alpha$ , are positively correlated  
31 22 to ALT. As both proteins are excreted, it is likely that they can be detected in the plasma and thus may be  
32 23 further investigated as potential diagnostic marker.

33 24 GLDH like ALT shows a strong initial response but in contrast to the latter as increases further up to  
34 25 18h, before it decreases gradually (Figure 8B). It is highly correlated to ALT, but shows a low correlation to  
35 26 all other factors (Figure 8B). In particular, the anti-correlation of GLDH to Cyp7a1, the 2nd highest  
36 27 correlation, is considerably lower than the ALT-Cyp7a1 correlation (see Supporting Information Dataset

4 S3, section 4.2). Further, it is correlated to RNA levels of Fibronectin (Fn1, see Figure 6G), but only in time  
5 frames including the 18h time point (T18h, 6-18h, Perp).

6  
7  
8 **9 Macroscopic organ damage**

10  
11 As documented with the H&E staining in Figure 2B, necroinflammation is caused by the BDL-induced  
12 intrahepatic toxic bile accumulation with individual liver cell death and progressive development of  
13 confluent bile infarct areas. The total area of infarcts increases steadily with relatively high variance  
14 (Figure 2A). The most consistently positively correlated factor with bile infarcts is plasma bilirubin, which  
15 occurs in most time frames and even at single time points (Figure 8C). The correlation is not very strong  
16 and the significance level is <5%, valid only for 3/11 time frames and 2/7 time points (see Supporting  
17 Information Dataset S3, section 4.10). The two parameters are biologically related as the infarct area  
18 inversely accounts for the number of functional hepatocytes.

19  
20 Next most correlated is the RNA level of Il17a encoding interleukin-17A (Figure 8C), which plays a  
21 pivotal role in cholestatic liver fibrosis in mice by activation of both the KCs and HSCs [19]. The correlation  
22 is high only for later time points. Il17a is switched on between 2d and 5d to very high RNA levels, and as it  
23 is a secreted protein, it is likely to be detectable in the blood, thus representing a candidate diagnostic  
24 marker. Expression of Notch3 is initially negatively and later positively correlated with bile infarcts. This  
25 corresponds to the pattern of Notch3 expression. It drops below the level of untreated mice and is  
26 increased between days 2 and 5. Notch3 is reported to be significantly up-regulated in fibrotic liver tissues,  
27 most supposedly by regulating the activation of HSCs [20]. Next, Prom1, encoding prominin 1 (CD133), is  
28 reported to be increased in alcoholic hepatitis [21] and chronic liver injury [22], and was dedicated to be  
29 regulated by the DNA methylation in HSCs [23]. Many of the selected genes were positively correlated to  
30 a similar extent, with the highest values occurring for the later time frames. Among those, Col3a1 (see  
31 Figure 6F), Sparc, Col8a1, Wisp1, and Edn1 show a similar pattern as Notch3 for the initial anti-  
32 correlation. Remarkably, all genes whose expression values have a high consensus correlation to the  
33 infarct area show a high correlation for the 5d time point and the time frames covering day 5, while there is  
34 low correlation for the earlier time points and frames (Figure 8C). In addition, 5 days is the time point with  
35 the highest variance of the infarct area (Figure 2A). This indicates that different routes of the disease  
36

4 process exist, defined by the infarct area at day 5 and marked by expression of genes such as Il17a,  
5 Notch3, Prom1, Col3a1 (see Figure 6F), Actb, Sparc, Tnc, and Tgfbr2.  
6  
7

8 **3 Loss of liver function**  
9

10  
11 There is a large variability of bilirubin levels among different mice from the same time point. As bile  
12 cannot leave the liver via the biliary system due to cholestasis, differences in the measured serum bilirubin  
13 show the capacity of the hepatocytes and the bile lakes to store conjugated bilirubin. The highest  
14 correlation with serum bilirubin levels can be observed for Tnfrsf1b, encoding tumor necrosis factor  
15 receptor 2 (Figure 8D). Next, a high correlation is found for Ccl2, encoding chemokine (C-C motif) ligand  
16 2, a soluble biomarker for hepatic fibrosis in NAFLD [24]. The 3rd highest correlation is found for Il10rb,  
17 encoding the interleukin 10 receptor β subunit, which was found up-regulated in NASH with fibrosis [25].  
18  
19 Intriguingly, the 12 factors most correlated to bilirubin levels show a negative correlation for the final time  
20 frame 14d (see Supporting Information Dataset S3, section 4.4). For instance, the mouse with the lowest  
21 bilirubin levels at day 14 (IM2, 9.12, see Supporting Information Dataset S1) has the highest Tnfrsf1b  
22 expression, leading to the hypothesis of alternate progression courses in the final disease stage.  
23  
24

25 Surprisingly, albumin synthesis is maintained relatively constant over the observation period of 14  
26 days (Figure 1D). Apparently, hepatic degradation of albumin is affected at similar levels as its synthesis.  
27  
28 Due to this finding, it is not surprising that albumin is poorly correlated to the dynamics of other factors  
29 investigated (Figure 8E). Cyp2b10 shows high correlations to Albumin only for separate time frames and  
30 time points.  
31  
32

33 **20 Hepatic cell proliferative response**  
34

35 In later phase of the disease process, different hepatic cells proliferate, underlined by co-  
36 immunostaining with BrdU and specific markers for hepatocytes, KC, and BECs (Figure 3), and indirectly  
37 reflected by the marked up-regulation of Ki67 mRNA (Figure 4A).  
38  
39

40 As compensatory activity of the liver to restore the damaged parenchyma, hepatocytes proliferate,  
41 monitored by the parameter BrdU-positive hepatocytes. It is markedly triggered between the 30h and 2d  
42 time point (Figure 3D). It is highly correlated with Mki67 expression (Figure 9B), encoding the antigen Ki-  
43 67, a known proliferation marker (Figure 9B). The 2nd highest correlated gene is Birc5, encoding survivin.  
44  
45

1 Yes-associated protein has been reported to regulate the hepatic response after bile duct ligation via  
2 modulation of survivin [28], underlining the role of survivin in hepatic tissue restructure. The 3rd highest  
3 correlation is found for Notch1, a transmembrane receptor involved in developmental processes, and its  
4 increase can as well be seen as a sign of cell plasticity and tissue restructuring. Next in line is Cdh2,  
5 encoding cadherin-2, which is normally associated to cancerous cells. The correlation is high at the time  
6 points 30h to 5d. Then Lama1, encoding laminin subunit  $\alpha$ -1, the next most correlated factor, follows an  
7 opposite pattern, as the correlation is high at early (6h) and late (2d-14d) time points. Lama1 was found to  
8 be increased in nonalcoholic fatty liver disease [29]. Further, Timp2, encoding tissue inhibitor of  
9 metalloproteinases 2, an antagonist for degradation of extracellular matrix (ECM), also correlates with the  
10 hepatocyte proliferative response and reflects increased ECM deposition and buildup of fibrotic tissue.

12 Liver macrophages infiltrate the liver tissue, are activated, and proliferate, monitored by the parameter  
13 "BrdU-positive Kupffer cells". This starts at 30 h in our time course to reach a maximum at day 2 and to  
14 decrease again thereafter (Figure 3E). There is no strong correlation with other parameters, yet the  
15 highest with Gsta2, encoding glutathione S-transferase A2 (Figure 9A), which facilitates bilirubin import  
16 [26]. The correlation is confined to the middle time points (30h-2d), the time frame of the strongest  
17 increase of KC proliferation, while in the beginning (6h-12h) and the end (5d-14d) a slight anti-correlation  
18 is found. The next highest correlation is to BrdU-positive BECs, again in the middle time frames (30h-2d),  
19 and with S100a4-positive cells, which itself has a higher correlation to BrdU-positive BECs. The same is  
20 true for the RNA level of the cell cycle gene Mki67. The factor Por, encoding cytochrome P450 reductase,  
21 is negatively correlated in the time frames and time point from 30h on, thus, resembles the up-and-down  
22 pattern inversely. Por is reported to be down-regulated in liver cirrhosis via the aryl hydrocarbon receptor  
23 AhR [27].

50 Also biliary epithelial cells (BEC) proliferate, monitored by the parameter "BrdU-positive BECs". The  
51 main increase occurs between days 2 and 5, where a minor increase can also be observed after 30 h  
52 (Figure 3A). Further, a remarkable variability of BEC proliferation in the different mice can be seen at day  
53 14. The highest correlation of this event is observed for the number of S100a4-positive cells (Figure 9C),  
54 which is representative for the number of KC and is in line with the recent finding about feed-forward and  
55 feedback regulation of the two cell types BEC and KC in liver fibrogenesis. Only the time frames near the  
56

4 perpetuation phase show a high correlation. Not surprisingly, the gene expression most correlated to  
5 BrdU-positive BECs was found for Col1a1 (Figures 9C and 6E), encoding the collagen deposited in ECM  
6 in large quantities. The 3<sup>rd</sup> highest correlation is found for Tgfb, encoding the cytokine TGFβ, which is well  
7 known to correspond with the fibrotic process in a positive feedback loop [30]. Interestingly, the negative  
8 correlation at the 6h time point shows high significance suggesting a negative feedback regulation. The 4<sup>th</sup>  
9 highest correlation is found for Il10rb, encoding the β-subunit for the Il10 receptor, which was described to  
10 be increased in rat liver fibrosis [31]. Slc10a1, encoding the Na<sup>+</sup>-taurocholate co-transporting polypeptide,  
11 which transports bile acids through the basolateral membranes of hepatocytes is negatively correlated  
12 with BEC proliferation, mainly in the later time frames (30h-14d). A decrease of Slc10a1 has been shown  
13 to protect hepatocytes from cholestasis-induced injury [32]. Another negatively correlated factor is Ugt1a1,  
14 encoding UDP-glucuronosyl-transferase 1A, the main enzyme for conjugation of bilirubin, whose down-  
15 regulation is considered protective against the increased concentration of conjugated bilirubin in  
16 hepatocytes.

17 **Increase in fibrogenic cells**

18 In accordance to the proliferative activity of HSCs, immunohistochemical analyses demonstrate the  
19 gradual rise in CTGF-, α-SMA- and S100a4-expressing cells (Figure 3), reflecting activated HSC,  
20 activated KC and trans-differentiated hepatocytes (such that they are producing hepatokines). CTGF is a  
21 highly pro-fibrogenic protein expressed by HSCs, BECs and hepatocytes [33; 34] and mediates  
22 extracellular matrix inducing properties. It is reported that levels of this protein are significantly up-  
23 regulated in experimental liver fibrogenesis and human chronic liver disease patients of various etiologies  
24 [35; 36]. The number of CTGF-positive show a steady increase with comparatively little variance (Figure  
25 3F), as shown by the high significances in ANOVA analysis (see Supplementary File 4). The highest  
26 correlation with CTGF positive cell number shows Tgfb2, encoding the cytokine TGF-β2 (Figures 9D and  
27 6I). TGF-β is the major stimulus for CTGF expression in hepatocytes [37] and elevated levels of Tgfb2  
28 were reported for bile duct ligated rats [38]. This is the result of a direct interaction [39], and the correlation  
29 is close to 1 for several time frames (30h-14d) and all time points, except for 30h. The next highest  
30 correlation is found for Pdgfb, encoding platelet-derived growth factor subunit B, which is reported to be

4 up-regulated in liver inflammation and fibrosis [40]. The number of cells containing CTGF and  $\alpha$ -SMA is  
5 also highly correlated. There is also a strong correlation to Tgfb2, encoding the transforming growth factor  
6  $\beta$  receptor 2 [41]. Additionally, there are considerable correlations to several other genes such as Timp1,  
7 Cxcl5, Sparc, and Col8a1.

8 The parameter “ $\alpha$ -SMA-positive cells”, a marker of HSC activation, increases steadily with the course  
9 of disease progression (Figure 3B). Not surprisingly, it is positively correlated to the number of CTGF-  
10 positive and S100a4-positive cells (Figure 9E). Interestingly, CTGF staining is highly anti-correlated to  
11 Cyp1a2 (Figure 6A), encoding cytochrome P450 1A2, known to be lowered in liver cirrhosis mediated by  
12 AhR [27]. The next most correlated gene is Pparg, encoding peroxisome proliferator-activated receptor  
13 gamma, but the most relevant correlation occurs in the early time frames, that is 18h-30h. PPAR- $\gamma$  inhibits  
14 HSC activation [42]. As Pparg is increasing only in the early stages, we conclude that TGF- $\beta$  and Pparg  
15 form a threshold system, where HSC activation is controlled in the first stage and overshooting in later  
16 time frames. Cyp2c37 shows a negative correlation in the early time frames (6h-18h), but the correlation  
17 of  $\alpha$ -SMA-positive cells to S100a4 is higher, as outlined below.

18 The S100a4 protein has been dedicated to myofibroblasts upon epithelial mesenchymal transition of  
19 hepatocytes in liver [43; 44]. This was however disproved in a careful analysis, indicating that the protein  
20 marks Kupffer cells [45]. The parameter “S100a4-positive cells” shows a steady rise until day 2, after  
21 which it stays constant (Figure 3C). Not surprisingly, it is positively correlated to the BrdU-positive BECs  
22 and  $\alpha$ -SMA-positive cells, but significant correlations do not occur after day 2 (Figure 9F). Expression of  
23 the gene Gstm1 (Figure 6C), encoding glutathione S-transferase Mu 1 is highly correlated. Genetic  
24 variation increases the susceptibility to alcoholic liver disease [46], but no connection between its  
25 regulation and other types of liver diseases has been reported. Cyp2c37 is negatively correlated,  
26 especially in the early time frames. The time course of Cyp2c37 expression shows a strong initial decline  
27 until 12 h, a plateau until day 2, and a final decline. Egfr, encoding epidermal growth factor receptor is also  
28 negatively correlated. Interestingly, both, but especially Egfr, show a higher anti-correlation for single time  
29 points than for time frames. Thus, although Egfr does not change much in the time course, it is a marker  
30 for increase of S100a4 positive cell number.

3  
4 **Fibrosis**

5 During the perpetuation phase (18h-2d), paracrine and autocrine cytokines amplify hepatic  
6 inflammation and HSC activation resulting in continued ECM remodeling, being characterized by the  
7 enhanced mRNA expression of both fibrillar collagen1 $\alpha$ 1 and 3 $\alpha$ 1 (Figures 6E and F). Additionally, the  
8 progression stage of fibrogenesis is histomorphologically characterized by excessive deposition of  
9 extracellular matrix (Figure 4B), as analyzed by Sirius red staining of liver slices (Figure 4C). Significant  
10 correlations of “Sirius red positive area” are found after day 2 (Figure 8F). The most correlated parameter  
11 is Osmr, encoding the oncostatin M receptor, which transduces, among others, Il13l and oncostatin  
12 signaling events. Interestingly, it has been reported that in cirrhotic liver, Osmr is not expressed [47]. Thus,  
13 expression of this gene may be a candidate distinguishing factor for liver cirrhosis and cholestasis-induced  
14 liver injury, which however has to be confirmed with further investigations. Also Osm, encoding oncostatin  
15 M itself, is correlated, showing a combined induction of the ligand and its receptor [48]. Next most  
16 correlated with Sirius red staining is Ccr5, encoding C-C chemokine receptor type 5, which is a regulator  
17 of inflammation as well as macrophage recruitment and trafficking [49], thus representing a general  
18 promoter of hepatic fibrosis [50]. Additionally, blood bilirubin levels are correlated, as described above.  
19 Further correlated factors are Tnfrsf1b, encoding tumor necrosis factor receptor 2, and Tnfrsf1a, encoding  
20 isoform 1 of the receptor (see Figure 6L). The latter was previously reported as necessary for liver fibrosis  
21 in mice [51]. Then Cxcr1, encoding interleukin 8 receptor  $\alpha$ , is reported to be highly up-regulated in  
22 chronic liver disease [52] and is found correlated with Sirius red (Figure 8F).

23  
24 **Markers of disease progression**

25 We next asked the question, which of the analyzed factors characterize particular stages of the  
26 disease process best. One-way ANOVA identifies the parameters whose values at different time points  
27 are different in a general perspective. The calculated p-values allow a ranking how good the parameters  
28 deviate in the time course, the top significant are: Cyp1a2, serum bilirubin, Il10rb, Tgfb1, Ccl2, Cd86,  
29 Ccr2, and Mrc1.

30 In a more specific analysis, parameters were identified which have the largest difference of values in  
31 a particular time frame, a consecutive series of time points or a single time point. A separator for a  
32

4 particular time frame is a parameter, whose value range for mice belonging to the respective time frame is  
5 disjoint from the value range of mice outside this time frame. The quality of a separator is measured by the  
6 distance between the ranges in relation to the full range, the separation gap (see Supporting Information  
7  
8 Dataset S3 for details).

9  
10 We identified 41 separators for specific time frames. For 35 of these separators, the values of the  
11 factor show a single transition, while for 6 separators, an internal time range is marked. 12 separators  
12 select a single time point, 9 of which separate the 0h time point (the control) from ligated mice. The  
13 transcript abundance for Nr0b2 (small heterodimer partner, SHP, see Figure 6D) is strongly decreased  
14 only for mice at the 6h time point. SHP is a repressor of retinoid and thyroid hormone, as well as estrogen  
15 receptors and by being diminished in human cirrhotic livers, it is suggested to be associated to cirrhosis  
16 and hepatic tumors [53]. This is also supported by the fact that cholestatic liver fibrosis induced by BDL  
17 was increased in SHP-/- mice [54]. Cyp24a1 (mitochondrial 1,25-dihydroxyvitamin D3 24-hydroxylase, see  
18 Figure 6B) is also a separator for the 6h time point, with a lower separation strength. It had been found  
19 increased in hepatoma cells [55]. Mmp10 (Stromelysin-2/transin-2, see Figure 6H) is a separator for the  
20 18h time point, the only other internal time point with such a separator in the investigated parameter set.  
21  
22 By degrading proteoglycans [56] and fibronectin [57], the metalloproteinase contributes to ECM break  
23 down [58] and is found increased after liver injury [57] and at intoxication [59]. The transcript of Cdh2  
24 (cadherin 2) has increased levels only for 6h and 12h. Il28b and Il2 (Figures 6J and K) display a similar  
25 pattern, but the separation gap is small.

26 Among the 9 separators for untreated mice (0h), serum ALT is the strongest separator. Serum  
27 bilirubin, Hmox1 (decycling heme oxygenase 1), and serum GLDH have a separation >1%, while  $\alpha$ -SMA-  
28 positive cells, Cxcl2 (chemokine (C-X-C motif) ligand 2), Cd14 (CD14 antigen), Timp1 (tissue inhibitor of  
29 metalloproteinase 1), and Mmp10 (Figure 6H) have smaller separation values.

30 CTGF-positive cell number is the separator with a large separation gaps for several time frames of  
31 transition (6h/12h, 12h/18h, 30h/2d, 5d/14d). Thus, it is clearly the best candidate from those selected to  
32 monitor the disease progress. It is also among the parameters with the highest ANOVA significance  
33 (which is particularly remarkable as only 3 could be analyzed compared to 5 for other parameters, See  
34 Supplementary File 4, section 1). S100a4-positive cells is a similarly good separator for two transitions

4 1 (12h/18h, 30h/2d). The parameter  $\alpha$ -SMA-positive cells is a good separator for the transitions 0h/6h,  
5 2 6h/12h, 12h/18h, thus it can be considered as the best marker for the initial disease process.

6 3 Cyp1a2 (cytochrome P450 1A2, Figure 6A) was identified as best separator for the 6h/12h transition,  
7 4 whereby transcript levels are initially high and steeply decrease between 6h and 12h. Cyp1a2 shows the  
8 5 highest significance in the ANOVA test, and parameters pairs with Cyp1a2 as one partner yield the  
9 6 highest significances in MANOVA tests which show its robustness as a marker, see Supplementary File 4.  
10 7 The gene product has already been observed to decrease upon bile obstruction [60]. The two other RNA  
11 8 separators for this transition (Cd14, Ccl2) are poor.

12 9 There are no suitable RNA markers for 12h/18h, 18h/30h and 30h/2d transitions. For the 18h/30h  
13 10 transition, there are no separators at all, which supports the definition of a perpetuation phase represented  
14 11 by the 18h and 30h time points. Strong separators are abundantly available for the 2d/5d transition, which  
15 12 indicates that large qualitative changes occur between day 2 and day 5 of the experimental disease  
16 13 process. The best separator is Il28b (interleukin 28B; Figures 11 and 6K). Based on this investigation, we  
17 14 conclude that transition from day 2 to day 5 can be easily monitored, also in clinical practice, as serum  
18 15 bilirubin is among the best separators, and the interleukins (Il28b, see Figure 6K, Il13, Il17a) as well as the  
19 16 growth factors (Pdgfb, Tgfb2, see Figure 6I, Hgf) and contributors to the extracellular matrix (SpaC,  
20 17 Col3a1, Col1a1, Figures 6F and E), all together encode excreted gene products, that should be detectable  
21 18 in blood samples. SpaC (secreted acidic cysteine rich glycoprotein), a known indicator of chronic liver  
22 19 disease [53] and a mediator of fibrosis [61], also has a large separation gap.

23 20 For the 5d/14d transition, CTGF-positive cell numbers and mRNA expression of Ctgf are the only  
24 21 separators, which is an argument in favor of the combination of the 5 and 14 day time point in the  
25 22 progression phase.

26 23 Figure 10 shows a summary of the disease processes, the serum factors or histopathological  
27 24 parameters they represent, and the most correlated factors.

28 25 **Decision trees to monitor disease progression**

29 26 Our next aim was to find combinations of factors allowing a prediction of the time after the ligation for  
30 27 a putative mouse. In a first approach a MANOVA combining two factors followed by a linear discriminant

4 analysis (LDA) was performed. The combination of the parameters CTGF cells and Cyp1a2 yields high  
5 recall of 0.88 in the leave-one-out cross-validation in the discriminant analysis, however, CTGF cells  
6 having only 3 repeats, violated the minimal requirement for MANOVA of this pair. The combination of  
7 Cyp1a2 and Tgfb1 obtained a recall of 0.72 and high significance. It shows, that these parameters along  
8 with other top scorers as Tnfrsf1a, Hk2, Fn1, Cyp3a11, Il1b, Il10rb are suitable marker candidates. See  
9 Supplementary File 4 for more information.

10  
11 However, using MANOVA and LDA with so few repeats is problematic. For instance, the check on  
12 normality of the parameter values for each time point is not reliable. Therefore we applied a more direct  
13 approach which uses fewer assumptions. As many factors possess disjoint value ranges at specific time  
14 points, an assessment with binary decision trees is possible where to each node a question is attached,  
15 whether a specific factor has a smaller or larger value than a given threshold value.

16  
17 Computationally, the decision tree is determined by the rule that the partial separator with the largest  
18 relative gap is used. A partial separator is a combination of a factor and a threshold value, which splits a  
19 time frame in subordinate time frames, if the respective value ranges are disjoint. The thresholds of the  
20 decision tree are defined as the median of the gap between the ranges. For a partial separator, it is  
21 sufficient to split a time frame (except for the root of the decision tree), e.g. ALT separates very well 0h  
22 from 6h (with respect to the time frame 0h-6h), although the values at 14d are similar to the values at 0h.  
23  
24 A partial separator is measured by the quotient of the gap range and the value range, the relative gap.

25  
26 The decision tree to predict the time point computed from all available data is shown in Figure 11A.  
27 This decision tree recalls the available data, i.e. the time point of every mouse is correctly predicted. It  
28 relies mainly on the factors CTGF- and  $\alpha$ -SMA-positive cells. This is consistent with data from other  
29 studies, which observed a correlation of increased CTGF levels with histological fibrosis stages [62; 63],  
30 suggesting CTGF as a valuable diagnostic target, since it can be measured in patients' blood and maybe  
31 used to follow-up on patients suffering from chronic liver diseases [64]. Other factors identified are  
32 Tnfrsf1a, Gstm1, and Il28b. Tnfrsf1a (tumor necrosis factor 1, see Figure 6L) aggravates steatohepatitis  
33 [65] and is essential for HSC proliferation and ECM remodeling [66]. Polymorphisms of Gstm1  
34 (glutathione-S-transferase mu 1, see Figure 6C) are a risk factor in alcoholic liver cirrhosis [67]. Il28b  
35

4 1 (interleukin 28 $\beta$ , see Figure 6K) polymorphisms are associated with fibrosis progression in patients with  
5 2 chronic hepatitis C [68].

6 3 As the decision trees are automatically generated, their predictive capacity can be tested with the  
7 4 leave-one-out approach. For each mouse in the experiment, a decision tree is generated under the  
8 5 exclusion of data from this mouse. Then, the decision tree is evaluated with the factor values of this  
9 6 mouse and compared with its true time point.

10 7 Doing so, 24 of 40 mice were not accountable by the decision tree, because the factors CTGF- and  $\alpha$ -  
11 8 SMA-positive cells used in all trees were only measured for 24 mice (3 of 5 repeats). Of the 24  
12 9 accountable mice, the predictions were correct for 15. For those 9 wrong predictions, the predicted time  
13 10 point was adjacent to the true time point. 4 of them misclassified between 18h and 30h, 3 between 2d and  
14 11 5d, one between 5d and 14d, as well as between 0h and 6h. The reason for misclassification is always an  
15 12 extreme value of the left out mouse.

16 13 As most of the misclassifications occurred between 18h and 30h, reliability is presumably improved if  
17 14 these time points are combined. Thus, for the next series of decision trees, phases instead of time points  
18 15 shall be predicted. As the histological factor “CTGF-positive cells” is the only separator between 18h and  
19 16 30h, decision trees for time points must use this factor, while for the prediction of phases, decision trees  
20 17 are possible that do not depend on histologic parameters.

21 18 The decision tree to predict the disease phase deduced from all available data is shown in Figure  
22 19 11B. IL28b and CTGF are contained as decision parameters, like in the decision tree for time points.  
23 20 Additionally, Fn1 (Fibronectin, see Figure 6G) is used, a constituent of the ECM in liver fibrosis. The leave-  
24 21 one-out approach yielded decision trees, for which 29 of 40 mice could be assessed because the  
25 22 parameter CTGF-positive cells was measured for the left out mouse. They predicted the phase for 28 of  
26 23 29 mice correctly. The wrong prediction was caused by the transcript value of IL10rb for the left-out mouse,  
27 24 which is far from the values of the other mice of the same time point, and the algorithm did not select this  
28 25 factor as a predictor for all other decision trees.

29 26 The histopathological factors (cell counts) were only measured only for 24 mice. After their exclusion,  
30 27 all 40 mice can be subjected to the leave-one-out test, in which 37 of 40 predictions were correct. Wrong  
31 28 predictions were the result of outlying values for Cyp1a2 (Figure 6A) and IL10rb (which were chosen as the  
32 29 30 31 32 33 34 35 36 37 38 39 40 41 42 43 44 45 46 47 48 49 50 51 52 53 54 55 56 57 58 59 60 61 62 63 64 65

4 decision factors for the decision tree in these cases), and the largest value for Cdh2. As cadherin is not  
5 excreted and presumably not suited as a serum marker, it was also excluded. Finally, a decision tree of  
6 IL28b, Fn1, and IL2 (Figures 6K, G, and J) was formed, genes whose gene products are likely to be  
7 excreted and more easily observable (Figure 11C). The leave-one-out test again yielded 37 of 40 correct  
8 predictions. See Supplementary File 3 for more details.

9  
10 **Alternate progression routes**

11 The large variation in the parameters infarct area (Figure 2) and collagen area (Figures 4B and C) in  
12 mice from the late experimental time points are an intriguing finding, considering the homogeneity of the  
13 experimental system. Indeed, they are negatively correlated with each other, and suggest that alternate  
14 routes of disease progression exist. One route is characterized by a strong increase in necrotic tissue and  
15 a weaker activation of HSC and lower expression change of inflammation factors. The other route is  
16 characterized by strong activation of fibrogenesis factors, and finally macroscopic collagen tissue. Both  
17 routes are similarly connected to loss of liver function, however, the histopathological display is quite  
18 different: the former contains a large amount of necrotic tissue while the latter contains large fibrotic  
19 tissue. Once verified also for human livers, the hypothesis of alternate disease routes can be of far-  
20 reaching importance for an individualized therapy, as obviously the medical interventions avoiding  
21 necrosis differ from interventions reducing overshooting fibrosis. The design of the study, which included  
22 the sacrifice of mice after a specific time, did not allow to answer whether the alternate developments,  
23 shown macroscopically in later time points, can also be observed in earlier time points.

24  
25 **Conclusion**

26 The time-resolved analysis of a wide range of parameters (6,313 in total) in bile duct ligated mice has  
27 shown that many factors share the pattern of an increase throughout disease progression (Figure 10),  
28 however, most of them display a large variability, which maybe the major reason why translation of a set  
29 of such parameters into diagnostic approaches have not proven sufficient robustness for valid predictions  
30 in human patients with chronic liver diseases. Count of CTGF-positive cells and expression of IL28b are  
31 among the few exceptions and their diagnostic potential is promising. The most correlated factor to CTGF-

4 positive cell numbers is TGF- $\beta$ 2 (Figure 6I). Both, CTGF and TGF- $\beta$ 2 encode excreted cytokines, and  
5 therefore represent good candidates as serum marker to monitor disease progression.  
6

7 For the regulatory program, the largest change of quality of the disease progress occurs between  
8 days 2 and 5, and is characterized by large expression changes of factors, such as IL2, IL28b or IL13. This  
9 information has strong clinical relevance, as it indicates a switching point, and human homologs of the  
10 respective interleukines are top candidates to be used as clinical markers.  
11

12 Our data suggest fibronectin (Fn1, Figure 6G) as the most sensitive marker for the onset of the  
13 disease process. Oncostatin M and its receptor are both highly correlated with the area of deposited  
14 collagen/ECM, suggesting it as a sensitive diagnostic marker for ongoing fibrogenesis.  
15

16 Our experiments also found previously unknown molecular events which are probably elements of a  
17 transcriptional program. For instance, there are strong transcript peaks for SHP (Nr0b2) at 6h or transin-2  
18 (Mmp10, Figure 6H) at 18h, which now need a focused analysis to delineate the chain of molecular  
19 interactions causing it and the functional consequences for disease onset and progression. This is a  
20 potential starting point in therapy.  
21

22 To conclude, a detailed time-resolved transcriptional profiling of liver homogenates following BDL  
23 revealed a coordinated induction of detoxification processes immediately after surgery and an up-  
24 regulation of an inflammatory response along with activation of metabolically active genes, which can be  
25 explained by physiological recovery and adaptation of the mice to the bile acid exposure.  
26

27 Based on our results, we propose binary decision trees from selected serum parameters, such as in  
28 Figure 11C as a promising tool for bedside assessment of disease progression. Therefore, as next step,  
29 suitability of the parameters selected from the mouse model need to be confirmed for human patients as  
30 in [69]. We additionally suggest to identify common transcription factors (TF)/TF-binding sites controlling  
31 the transcription of those genes with the most significantly correlated expression.  
32

## 33 24 Availability of supporting data 34

35 25 The data sets supporting the results of this article are included within the article and its additional files.  
36

37 26 Dataset S1. Measurements in bile duct ligated mice.  
38

39 27 Dataset S2. Correlations of factors.  
40

- 4   1 Dataset S3. Separators and decision trees.  
5  
6   2 Dataset S4. Detailed account on significance calculations.  
7  
8

9   3 **List of Abbreviations**  
10  
11

12   4 CTGF: connective tissue growth factor; BDL: bile duct ligation; SHP: small heterodimer partner; CLD:  
13   5 chronic liver disease; HSC: hepatic stellate cells; KC: Kupffer cells; ADME: absorption, distribution,  
14   6 metabolism, and excretion; ALT: alanine aminotransferase; GLDH: glutamate dehydrogenase; EDTA:  
15   7 ethylenediaminetetraacetic acid; H&E: hematoxylin and eosin;  
16  
17

18   8  
19  
20   9 **Competing Interests**  
21  
22

23   10 The authors declare that they have no conflicts of interest.  
24  
25

26   11  
27  
28   12 **Author Contributions**  
29  
30

31   13 Conceived and designed the experiments: KA AH MT IM BV SD. Performed the experiments: KA MT IM  
32   14 HW. Analyzed the data: KA AH MT IM ME HW HH UMZ BV SD. Wrote the paper: KA AH MT ME HW HH  
33  
34   15 UMZ BV SD. All authors read and approved the final manuscript.  
35  
36

37   16 **Acknowledgments**  
38  
39

40   17 The authors kindly thank Dorothea Frenz, Berit Blendow, Maren Nerowski, Doris Butzlaff and Eva  
41  
42   18 Lorbeer-Rehfeldt (Institute for Experimental Surgery, University of Rostock) and Igor Liebermann (Institute  
43  
44   19 of Clinical Pharmacology, Stuttgart) for their excellent technical assistance. The study was supported by  
45  
46   20 grants from the German Research Foundation to Kerstin Abshagen (AB 453/1-1), by the BMBF program  
47  
48   21 "Virtual Liver" (Grants 0315755, 0315764) and by the Robert Bosch Foundation, Stuttgart, Germany. The  
49  
50   22 funders had no role in study design, data collection and analysis, decision to publish, or preparation of the  
51  
52   23 manuscript.  
53  
54

55   24  
56  
57  
58  
59  
60  
61  
62  
63  
64  
65

5 **References**

- 6
- 7 1. Rockey DC. Translating an understanding of the pathogenesis of hepatic fibrosis to novel therapies.  
8 2. Clin Gastroenterol Hepatol. 2013;11:224-31.
- 9 3. Diehl AM, Chute J. Underlying potential: cellular and molecular determinants of adult liver repair. J  
10 4. Clin Invest. 2013;123:1858-60.
- 11 5. Schuppan D, Kim YO. Evolving therapies for liver fibrosis. J Clin Invest. 2013;123:1887-1901.
- 12 6. An G, Mi Q, Dutta-Moscatom J, Vodovotz Y. Agent-based models in translational systems biology.  
13 7. Wiley Interdiscip Rev Syst Biol Med. 2009; 1:159-71.
- 14 8. Georgiev P, Jochum W, Heinrich S, Jang JH, Nocito A, Dahm F, et al. Characterization of time-  
15 9. related changes after experimental bile duct ligation. Br J Surg. 2008;95:646-56.
- 16 10. Spurgeon SL, Jones RC, Ramakrishnan R. High throughput gene expression measurement with real  
17 11. time PCR in a microfluidic dynamic array. PLoS One. 2008;3:e1662.
- 18 12. Geerts AM, Vanheule E, Praet M, Van Vlierberghe H, De Vos M, Colle I. Comparison of three  
19 13. research models of portal hypertension in mice: macroscopic, histological and portal pressure  
20 14. evaluation. Int J Exp Pathol. 2008;89:251-63.
- 21 15. Kisseeleva T, Brenner DA. Anti-fibrogenic strategies and the regression of fibrosis. Best Pract Res  
22 16. Clin Gastroenterol. 2011;25:305-17.
- 23 17. Mederacke I, Hsu CC, Troeger JS, Huebener P, Mu X, Dapito DH, et al. Fate tracing reveals hepatic  
24 18. stellate cells as dominant contributors to liver fibrosis independent of its aetiology. Nat Commun.  
25 19. 2013;4:2823.
- 26 20. Holt AP, Salmon M, Buckley CD, Adams DH. Immune interactions in hepatic fibrosis. Clin Liver Dis.  
27 21. 2008;12:861-82.
- 28 22. Wasmuth HE, Lammert F, Zaldivar MM, Weiskirchen R, Hellerbrand C, Scholten D, et al. Antifibrotic  
29 23. effects of CXCL9 and its receptor CXCR3 in livers of mice and humans. Gastroenterology.  
30 24. 2009;137:309-19.
- 31 25. Heinrichs D, Berres ML, Nellen A, Fischer P, Scholten D, Trautwein C, et al. The chemokine CCL3  
32 26. promotes experimental liver fibrosis in mice. PLoS One. 2013;8:e66106.
- 33 27.

- 4 13. Leask A, Abraham DJ. All in the CCN family: essential matricellular signaling modulators emerge  
5 from the bunker. *J Cell Sci.* 2006;119:4803-10.  
6  
7 14. Gressner AM, Weiskirchen R, Breitkopf K, Dooley S. Roles of TGF-beta in hepatic fibrosis. *Front  
8 Biosci.* 2002;7:d793-807.  
9  
10 15. Gupta S, Stravitz RT, Dent P, Hylemon PB. Down-regulation of cholesterol 7alpha-hydroxylase  
11 (CYP7A1) gene expression by bile acids in primary rat hepatocytes is mediated by the c-Jun N-  
12 terminal kinase pathway. *J Biol Chem.* 2001;276:15816-22.  
13  
14 16. Russell DW. Nuclear orphan receptors control cholesterol catabolism. *Cell.* 1999;97:539-42.  
15  
16 17. Schacter BA, Joseph E, Firneisz G. Effect of cholestasis produced by bile duct ligation on hepatic  
17 heme and hemoprotein metabolism in rats. *Gastroenterology.* 1983;84:227-35.  
18  
19 18. Hattori T, Ohoka N, Hayashi H, Onozaki K. C/EBP homologous protein (CHOP) up-regulates IL-6  
20 transcription by trapping negative regulating NF-IL6 isoform. *FEBS Lett.* 2003;541:33-9.  
21  
22 19. Hara M, Kono H, Furuya S, Hirayama K, Tsuchiya M, Fujii H. Interleukin-17A plays a pivotal role in  
23 cholestatic liver fibrosis in mice. *J Surg Res.* 2013;183:574-82.  
24  
25 20. Chen YX, Weng ZH, Zhang SL. Notch3 regulates the activation of hepatic stellate cells. *World J  
26 Gastroenterol.* 2012;18:1397-403.  
27  
28 21. Sancho-Bru P, Altamirano J, Rodrigo-Torres D, Coll M, Millán C, José Lozano J, et al. Liver  
29 progenitor cell markers correlate with liver damage and predict short-term mortality in patients with  
30  
31 41 alcohol hepatitis. *Hepatology.* 2012;55:1931-41.  
32  
33 22. Fujii T, Fuchs BC, Yamada S, Lauwers GY, Kulu Y, Goodwin JM, et al. Mouse model of carbon  
34 tetrachloride induced liver fibrosis: Histopathological changes and expression of CD133 and  
35 epidermal growth factor. *BMC Gastroenterol.* 2010;10:79.  
36  
37 23. Reister S, Kordes C, Sawitsa I, Häussinger D. The epigenetic regulation of stem cell factors in  
38 hepatic stellate cells. *Stem Cells Dev.* 2011;20:1687-99.  
39  
40 24. Page S, Birerdinc A, Estep M, Stepanova M, Afendy A, Petricoin E, et al. Knowledge-based  
41 identification of soluble biomarkers: hepatic fibrosis in NAFLD as an example. *PLoS One.*  
42  
43 27 2013;8:e56009.  
44  
45  
46  
47  
48  
49  
50  
51  
52  
53  
54  
55  
56  
57  
58  
59  
60  
61  
62  
63  
64  
65

- 4 1 25. Estep JM, Baranova A, Hossain N, Elariny H, Ankrah K, Afendy A, et al. Expression of cytokine  
5 2 signaling genes in morbidly obese patients with non-alcoholic steatohepatitis and hepatic fibrosis.  
6 3 *Obes Surg.* 2009;19:617-24.
- 7 4 26. Huang W, Zhang J, Chua SS, Qatanani M, Han Y, Granata R, et al. Induction of bilirubin clearance  
8 5 by the constitutive androstane receptor (CAR). *Proc Natl Acad Sci U S A.* 2003;100:4156-61.
- 9 6 27. Floreani M, De Martin S, Gabbia D, Barbierato M, Nassi A, Mescoli C, et al. Severe liver cirrhosis  
10 7 markedly reduces AhR-mediated induction of cytochrome P450 in rats by decreasing the  
11 8 transcription of target genes. *PLoS One.* 2013;8:e61983.
- 12 9 28. Bai H, Zhang N, Xu Y, Chen Q, Khan M, Potter JJ, et al. Yes-associated protein regulates the  
13 10 hepatic response after bile duct ligation. *Hepatology.* 2012;56:1097-107.
- 14 11 29. Sookoian S, Gianotti TF, Rosselli MS, Burgueño AL, Castaño GO, Pirola CJ. Liver transcriptional  
15 12 profile of atherosclerosis-related genes in human nonalcoholic fatty liver disease. *Atherosclerosis.*  
16 13 2011;218:378-85.
- 17 14 30. Inagaki Y, Okazaki I. Emerging insights into Transforming growth factor beta Smad signal in hepatic  
18 15 fibrogenesis. *Gut.* 2007;56:284-92.
- 19 16 31. Rachmawati H, Beljaars L, Reker-Smit C, Van Loenen-Weemaes AM, Hagens WI, Meijer DK, et al.  
20 17 Pharmacokinetic and biodistribution profile of recombinant human interleukin-10 following  
21 18 intravenous administration in rats with extensive liver fibrosis. *Pharm Res.* 2004;21:2072-8.
- 22 19 32. Eipel C, Menschikow E, Sigal M, Kuhla A, Abshagen K, Vollmar B. Hepatoprotection in bile duct  
23 20 ligated mice mediated by darbepoetin- $\alpha$  is not caused by changes in hepatobiliary transporter  
24 21 expression. *Int J Clin Exp Pathol.* 2013;6:80-90.
- 25 22 33. Paradis V, Dargere D, Vidaud M, De Gouville AC, Huet S, Martinez V, et al. Expression of  
26 23 connective tissue growth factor in experimental rat and human liver fibrosis. *Hepatology.*  
27 24 1999;30:968-76.
- 28 25 34. Sedlacek N, Jia JD, Bauer M, Herbst H, Ruehl M, Hahn EG, et al. Proliferating bile duct epithelial  
29 26 cells are a major source of connective tissue growth factor in rat biliary fibrosis. *Am J Pathol.*  
30 27 2001;158:1239-44.

- 4 1 35. Rachfal AW, Brigstock DR. Connective tissue growth factor (CTGF/CCN2) in hepatic fibrosis.  
5 2 Hepatol Res. 2003;26:1-9.
- 6 3 36. Dendooven A, Gerritsen KG, Nguyen TQ, Kok RJ, Goldschmeding R. Connective tissue growth  
7 4 factor (CTGF/CCN2) ELISA: a novel tool for monitoring fibrosis. Biomarkers. 2011;16:289-301.
- 8 5 37. Liu Y, Liu H, Meyer C, Li J, Nadalin S, Königsrainer A, et al. Transforming growth factor- $\beta$  (TGF- $\beta$ )-  
9 6 mediated connective tissue growth factor (CTGF) expression in hepatic stellate cells requires Stat3  
10 7 signaling activation. J Biol Chem. 2013;288:30708-19.
- 11 8 38. Schierwagen R, Leeming DJ, Klein S, Granzow M, Nielsen MJ, Sauerbruch T, et al. Serum markers  
12 9 of the extracellular matrix remodeling reflect antifibrotic therapy in bile-duct ligated rats. Front  
13 10 Physiol. 2013;4:195.
- 14 11 39. Wang Q, Usinger W, Nichols B, Gray J, Xu L, Seeley TW, et al. Cooperative interaction of CTGF  
15 12 and TGF- $\beta$  in animal models of fibrotic disease. Fibrogenesis Tissue Repair. 2011;4:4.
- 16 13 40. Malizia G, Brunt EM, Peters MG, Rizzo A, Broekelmann TJ, McDonald JA. Growth factor and  
17 14 procollagen type I gene expression in human liver disease. Gastroenterology. 1995;108:145-56.
- 18 15 41. Yang L, Inokuchi S, Roh YS, Song J, Loomba R, Park EJ, et al. Transforming growth factor- $\beta$   
19 16 signaling in hepatocytes promotes hepatic fibrosis and carcinogenesis in mice with hepatocyte-  
20 17 specific deletion of TAK1. Gastroenterology. 2013;144:1042-54.
- 21 18 42. Qian J, Niu M, Zhai X, Zhou Q, Zhou Y.  $\beta$ -Catenin pathway is required for TGF- $\beta$ 1 inhibition of  
22 19 PPAR $\gamma$  expression in cultured hepatic stellate cells. Pharmacol Res. 2012;66:219-25.
- 23 20 43. Zeisberg M, Yang C, Martino M, Duncan MB, Rieder F, Tanjore H, et al. Fibroblasts derive from  
24 21 hepatocytes in liver fibrosis via epithelial to mesenchymal transition. J Biol Chem. 2007;282:23337-  
25 22 47.
- 26 23 44. Robertson H, Kirby JA, Yip WW, Jones DE, Burt AD. Biliary epithelial-mesenchymal transition in  
27 24 posttransplantation recurrence of primary biliary cirrhosis. Hepatology. 2007;45:977-81.
- 28 25 45. Österreicher CH, Penz-Österreicher M, Grivennikov SI, Guma M, Koltsova EK, Datz C, et al.  
29 26 Fibroblast-specific protein 1 identifies an inflammatory subpopulation of macrophages in the liver.  
30 27 Proc Natl Acad Sci U S A. 2011;108:308-13.

- 4 1 46. Baclig MO, Alvarez MR, Lozada XM, Mapua CA, Lozano-Kühne JP, Dimamay MP, et al. Association  
5 2 of glutathione S-transferase T1 and M1 genotypes with chronic liver diseases among Filipinos. *Int J*  
6 3 *Mol Epidemiol Genet.* 2012;3:153-9.
- 7 4 47. Znoyko I, Sohara N, Spicer SS, Trojanowska M, Reuben A. Expression of oncostatin M and its  
8 5 receptors in normal and cirrhotic human liver. *J Hepatol.* 2005;43:893-900.
- 9 6 48. Liang H, Block TM, Wang M, Nefsky B, Long R, Hafner J, et al. Interleukin-6 and oncostatin M are  
10 7 elevated in liver disease in conjunction with candidate hepatocellular carcinoma biomarker GP73.  
11 8 *Cancer Biomark.* 2012;11:161-71.
- 12 9 49. Barashi N, Weiss ID, Wald O, Wald H, Beider K, Abraham M, et al. Inflammation-induced  
13 10 hepatocellular carcinoma is dependent on CCR5 in mice. *Hepatology.* 2013;58:1021-30.
- 14 11 50. Seki E, De Minicis S, Gwak GY, Kluwe J, Inokuchi S, Bursill CA, et al. CCR1 and CCR5 promote  
15 12 hepatic fibrosis in mice. *J Clin Invest.* 2009;119:1858-70.
- 16 13 51. Sudo K, Yamada Y, Moriwaki H, Saito K, Seishima M. Lack of tumor necrosis factor receptor type 1  
17 14 inhibits liver fibrosis induced by carbon tetrachloride in mice. *Cytokine.* 2005;29:236-44.
- 18 15 52. Zimmermann HW, Seidler S, Gassler N, Nattermann J, Luedde T, Trautwein C, et al. Interleukin-8 is  
19 16 activated in patients with chronic liver diseases and associated with hepatic macrophage  
20 17 accumulation in human liver fibrosis. *PLoS One.* 2011;6:e21381.
- 21 18 53. Smalling RL, Delker DA, Zhang Y, Nieto N, McGuiness MS, Liu S, et al. Genome-wide transcriptome  
22 19 analysis identifies novel gene signatures implicated in human chronic liver disease. *Am J Physiol*  
23 20 *Gastrointest Liver Physiol.* 2013;305:G364-74.
- 24 21 54. Zhang Y, Xu N, Xu J, Kong B, Copple B, Guo GL, et al. E2F1 is a novel fibrogenic gene that  
25 22 regulates cholestatic liver fibrosis through the Egr-1/SHP/EID1 network. *Hepatology.* 2014;60:919-  
26 23 30.
- 27 24 55. Horvath E, Lakatos P, Balla B, Kósa JP, Tóbiás B, Jozilan H, et al. Marked increase of CYP24A1  
28 25 mRNA level in hepatocellular carcinoma cell lines following vitamin D administration. *Anticancer*  
29 26 *Res.* 2012;32:4791-6.
- 30 27 56. Fosang AJ, Neame PJ, Hardingham TE, Murphy G, Hamilton JA. Cleavage of cartilage proteoglycan  
31 28 between G1 and G2 domains by stromelysins. *J Biol Chem.* 1991;266:15579-82.

- 4 1 57. Garcia-Irigoyen O, Carotti S, Latasa MU, Uriarte I, Fernández-Barrena MG, Elizalde M, et al. Matrix  
5 2 metalloproteinase-10 expression is induced during hepatic injury and plays a fundamental role in  
6 3 liver tissue repair. *Liver Int.* 2014;34:e257-70.  
7  
8 4 58. Krampert M, Bloch W, Sasaki T, Bugnon P, Rülicke T, Wolf E, et al. Activities of the matrix  
9 5 metalloproteinase stromelysin-2 (MMP-10) in matrix degradation and keratinocyte organization in  
10 6 wounded skin. *Mol Biol Cell.* 2004;15:5242-54.  
11  
12 7 59. LaFramboise WA, Bombach KL, Pogozelski AR, Cullen RF, Muha N, Lyons-Weiler J, et al. Hepatic  
13 8 gene expression response to acute indomethacin exposure. *Mol Diagn Ther.* 2006;10:187-96.  
14  
15 9 60. Fukushima S, Okuno H, Shibatani N, Nakahashi Y, Seki T, Okazaki K. Effect of biliary obstruction  
16 10 and internal biliary drainage on hepatic cytochrome P450 isozymes in rats. *World J Gastroenterol.*  
17 11 2008;14:2556-60.  
18  
19 12 61. Trombetta-Esilia J, Bradshaw AD. The function of SPARC as a mediator of fibrosis. *Open*  
20 13 *Rheumatol J.* 2012;6:146-155.  
21  
22 14 62. Hayashi N, Kakimura T, Soma Y, Grotendorst GR, Tamaki K, Harada M, et al. Connective tissue  
23 15 growth factor is directly related to liver fibrosis. *Hepatogastroenterology.* 2002;49:133-5.  
24  
25 16 63. Colak Y, Senates E, Coskunpinar E, Oltulu YM, Zemheri E, Ozturk O, et al. Concentrations of  
26 17 connective tissue growth factor in patients with nonalcoholic fatty liver disease: association with liver  
27 18 fibrosis. *Dis Markers.* 2012;33:77-83.  
28  
29 19 64. Gressner OA, Fang M, Li H, Lu LG, Gressner AM, Gao CF. Connective tissue growth factor  
30 20 (CTGF/CCN2) in serum is an indicator of fibrogenic progression and malignant transformation in  
31 21 patients with chronic hepatitis B infection. *Clin Chim Acta.* 2013;421:126-31.  
32  
33 22 65. Aparicio-Vergara M, Hommelberg PP, Schreurs M, Gruben N, Stienstra R, Shiri-Sverdlov R, et al.  
34 23 Tumor necrosis factor receptor 1 gain-of-function mutation aggravates nonalcoholic fatty liver  
35 24 disease but does not cause insulin resistance in a murine model. *Hepatology.* 2013;57:566-76.  
36  
37 25 66. Tarrats N, Moles A, Morales A, García-Ruiz C, Fernández-Checa JC, Marí M. Critical role of tumor  
38 26 necrosis factor receptor 1, but not 2, in hepatic stellate cell proliferation, extracellular matrix  
39 27 remodeling, and liver fibrogenesis. *Hepatology.* 2011;54:319-27.  
40  
41  
42  
43  
44  
45  
46  
47  
48  
49  
50  
51  
52  
53  
54  
55  
56  
57  
58  
59  
60  
61  
62  
63  
64  
65

- 4 1 67. Khan AJ, Choudhuri G, Husain Q, Parmar D. Polymorphism in glutathione-S-transferases: a risk  
5 factor in alcoholic liver cirrhosis. *Drug Alcohol Depend.* 2009;101:183-90.  
6 2  
7 3 68. Noureddin M, Wright EC, Alter HJ, Clark S, Thomas E, Chen R, et al. Association of IL28B genotype  
8 with fibrosis progression and clinical outcomes in patients with chronic hepatitis C: a longitudinal  
9 analysis. *Hepatology.* 2013;58:1548-57.  
10 4  
11 5  
12 6 69. Gadd VL, Skoien R, Powell EE, Fagan KJ, Winterford C, Horsfall L, et al. The portal inflammatory  
13 7 infiltrate and ductular reaction in human nonalcoholic fatty liver disease. *Hepatology.* 2014;59:1393-  
14 8 1405.  
15 9

22  
23  
24  
25  
26  
27  
28  
29  
30  
31  
32  
33  
34  
35  
36  
37  
38  
39  
40  
41  
42  
43  
44  
45  
46  
47  
48  
49  
50  
51  
52  
53  
54  
55  
56  
57  
58  
59  
60  
61  
62  
63  
64  
65

6 **Tables**  
7  
89 **Table 1.** Analysis of systemic blood cell count of sham-operated mice (S) and mice underwent BDL.  
10  
1112 Values are given as means  $\pm$  SEM.  
13  
14

	erythrocytes	platelets	leukocytes	hemoglobin	hematocrit
<b>S</b>	8.4 $\pm$ 0.1	1177 $\pm$ 60	7.5 $\pm$ 0.3	7.9 $\pm$ 0.1	44.8 $\pm$ 0.7
<b>6h</b>	8.1 $\pm$ 0.1	1061 $\pm$ 39	4.2 $\pm$ 0.5	7.7 $\pm$ 0.1	42.8 $\pm$ 0.7
<b>12h</b>	8.2 $\pm$ 0.1	1036 $\pm$ 47	4.5 $\pm$ 0.4	7.7 $\pm$ 0.1	43.0 $\pm$ 0.6
<b>18h</b>	8.7 $\pm$ 0.3	856 $\pm$ 110	4.1 $\pm$ 0.2	8.1 $\pm$ 0.3	45.6 $\pm$ 1.9
<b>30h</b>	8.5 $\pm$ 0.5	1071 $\pm$ 100	5.8 $\pm$ 0.9	7.9 $\pm$ 0.5	44.9 $\pm$ 2.8
<b>2d</b>	8.7 $\pm$ 0.2	1117 $\pm$ 65	4.7 $\pm$ 1.3	6.5 $\pm$ 1.7	45.9 $\pm$ 0.9
<b>5d</b>	8.7 $\pm$ 0.3	1295 $\pm$ 107	7.6 $\pm$ 1.2	7.8 $\pm$ 0.3	46.5 $\pm$ 1.6
<b>14d</b>	7.6 $\pm$ 1.4	1362 $\pm$ 58	7.4 $\pm$ 1.1	6.6 $\pm$ 0.2	38.4 $\pm$ 1.3

3  
4 **Figure legends**5  
6  
7 **Figure 1: Analysis of liver injury and-function.** Plasma activities of alanine aminotransferase (ALT) (**A**)  
8 and glutamate dehydrogenase (GLDH) (**B**) and concentrations of plasma bilirubin (**C**) and albumin (**D**) at  
9 multiple time points after BDL. Values are given in means  $\pm$  SEM of five independent experiments per time  
10 point.  
11  
12  
13  
1415  
16  
17 **Figure 2: Quantification of bile infarcts at multiple time points after BDL (A).** Values are given in  
18 means  $\pm$  SEM of five independent experiments per time point. Representative H&E stainings of paraffin-  
19 embedded liver sections for each time point after BDL (**B**; arrows indicate bile lakes; magnification x10)  
20 with higher magnifications (x40) in (**C**), displaying cellular infiltrates (asterisk) and formation of artificial bile  
21 ductules (arrowhead).  
22  
23  
24  
25  
2627  
28  
29 **Figure 3: Analysis of the proliferative and cellular response at multiple time points after BDL.**  
30 Quantitative immunohistochemical analysis of BrdU-positive biliary epithelial cells (**A**), liver cells positive  
31 for  $\alpha$ -SMA (**B**) and S100a4 (**C**), BrdU-positive hepatocytes (**D**) and Kupffer cells (**E**) and CTGF-positive  
32 cells (**F**). Values are given in means  $\pm$  SEM of five independent experiments per time point.  
33 Corresponding representative immunohistochemical stainings are shown in the right panel (magnifications  
34 x40).  
35  
36  
37  
38  
39  
4041  
42  
43 **Figure 4: Analysis of proliferation and extracellular matrix accumulation.** mRNA quantification of the  
44 proliferation marker Ki67 (**A**) by Fluidigm real-time PCR. Values are given in means  $\pm$  SD of five  
45 independent experiments per time point. Quantitative analysis (**B**) and representative histological images  
46 (**C**; magnification x10) of Sirius red-positive areas at multiple time points after BDL. Values are given in  
47 means  $\pm$  SEM of five independent experiments per time point.  
48  
49  
50  
51  
52  
53  
54  
5556 **Figure 5: Heat maps displaying gene expression pattern at multiple time points after BDL.** Gene  
57 expression relative to Gapdh gene, obtained from Fluidigm qPCR, are shown as fold changes to sham  
58

4 mice. Red colour indicates up-regulation, blue down-regulation and white transcription levels about 1. (A)  
5 selected ADME genes, (B) selected fibrogenesis genes, and (C) selected cytokine genes.  
6  
7  
8  
9

10 **Figure 6: mRNA quantification of different genes by Fluidigm real-time PCR.** (A) Cyp1a2, (B)  
11 Cyp24a1, (C) Gstm1, (D) Nr0b2, (E) Col1 $\alpha$ 1, (F) Col3 $\alpha$ 1, (G), Fn1, (H) Mmp10, (I) Tgfb2, (J) Il2, (K) Il28b,  
12 (L) Tnfrsf1a. Values are given in means  $\pm$  SEM of five independent experiments per time point.  
13  
14  
15  
16  
17

18 **Figure 7: Clusters of consensus correlations.** The dendrogram represents the level of correlation.  
19 Factors connected near the periphery are highly correlated, whereas factors separated near the center  
20 have low correlation. The color of the factors show a set of 30 clusters based on the hierarchical cluster  
21 tree.  
22  
23  
24  
25  
26  
27  
28

29 **Figure 8: Correlations of ALT (A), GLDH (B), bile infarcts (C), bilirubin (D), albumin (E) and Sirius red (F)**  
30 with other factors as heat map. The right panel shows the correlations of and with other factors as heat  
31 map. The shade of the red and blue represents the correlation, where blue shows anti-correlation. The  
32 significance is shown as the shade of yellow below the correlation color segment, where darker shades  
33 lower p-values in the t-test. The shade of green represents the consensus correlation. In the Supporting  
34 Information Dataset S1, this data is shown with explicit numbers, see also the scale.  
35  
36  
37  
38  
39  
40  
41  
42  
43  
44  
45  
46  
47  
48  
49  
50  
51  
52  
53  
54  
55  
56  
57  
58  
59  
60  
61  
62  
63  
64  
65

20 **Figure 9: Correlations of BrdU-positive Kupffer cells (A), hepatocytes (B), biliary epithelial cells (C),**  
21 CTGF-positive cells (D),  $\alpha$ -SMA-positive cells (E) and S100a4-positive (F) with other factors as heat map.  
22 The right panel shows the correlations of and with other factors as heat map. The shade of the red and  
23 blue represents the correlation, where blue shows anti-correlation. The significance is shown as the shade  
24 of yellow below the correlation color segment, where darker shades lower p-values in the t-test. The  
25 shade of green represents the consensus correlation. In the Supporting Information Dataset S2, this data  
26 is shown with explicit numbers.  
27  
28  
29  
30  
31  
32  
33  
34  
35  
36  
37  
38  
39  
40  
41  
42  
43  
44  
45  
46  
47  
48  
49  
50  
51  
52  
53  
54  
55  
56  
57  
58  
59  
60  
61  
62  
63  
64  
65

4   **Figure 10: Outline of the disease process.** Each box is dedicated to a specific disease aspect (first line)  
5   which is represented by a commonly known marker (second line) or several markers. Below (in small font)  
6   the genes are shown whose expression is correlated to the factor above, mostly novel putative markers  
7   obtained from our analysis.  
8  
9

10   5  
11  
12   **Figure 11: Decision trees.** Decision trees for the prediction of time points (**A**) and disease phases (**B** and  
13   7  
14   **C**), where the latter shows the decision tree with the exclusion of histological factors.  
15  
16   8  
17  
18  
19  
20  
21  
22  
23  
24  
25  
26  
27  
28  
29  
30  
31  
32  
33  
34  
35  
36  
37  
38  
39  
40  
41  
42  
43  
44  
45  
46  
47  
48  
49  
50  
51  
52  
53  
54  
55  
56  
57  
58  
59  
60  
61  
62  
63  
64  
65

**Figure 1**

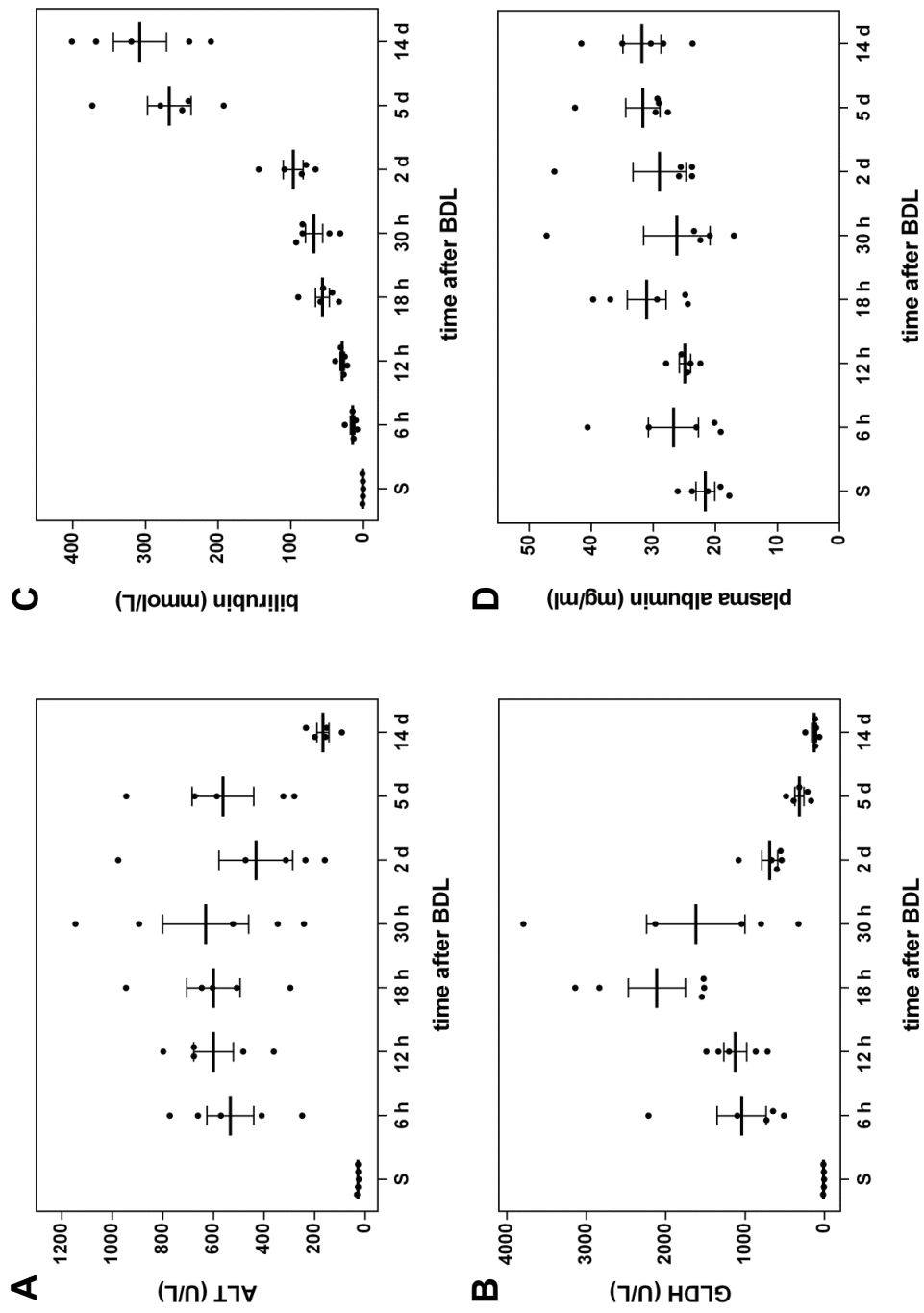


**Figure 2**

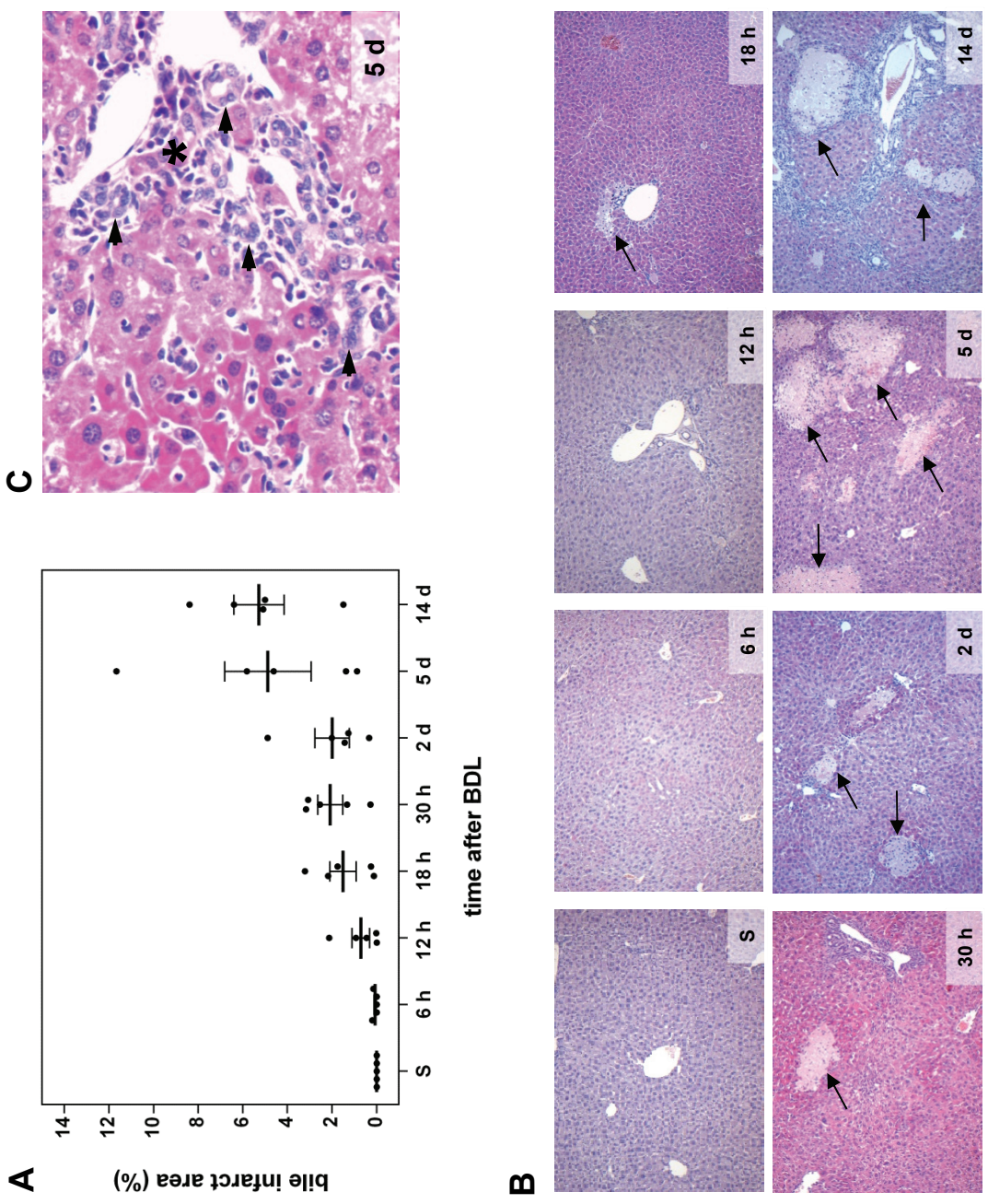
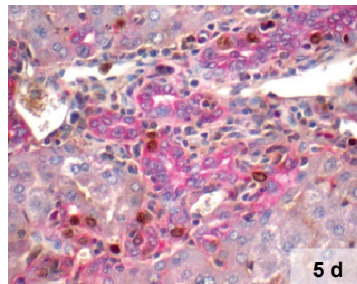
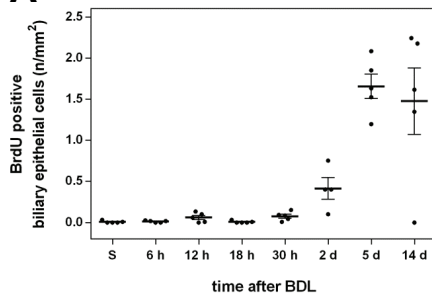
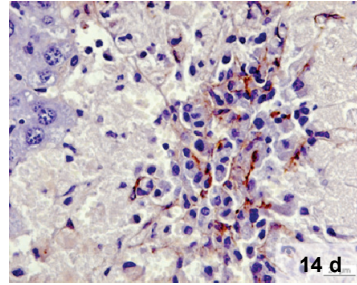
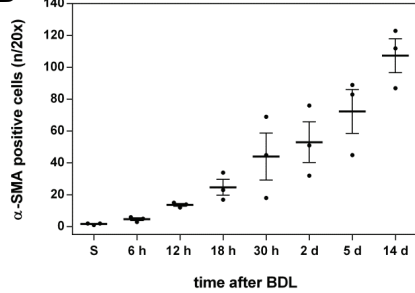


# Figure 3

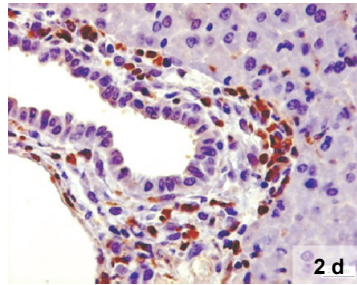
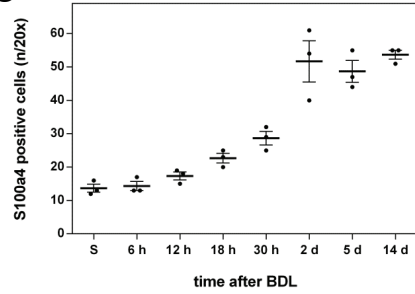
A



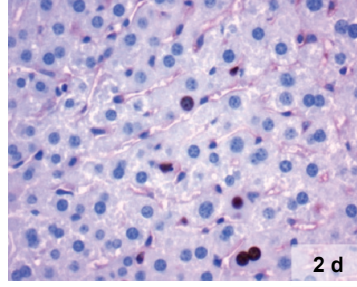
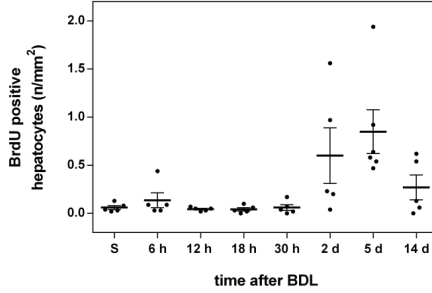
B



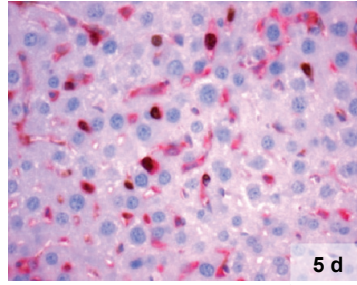
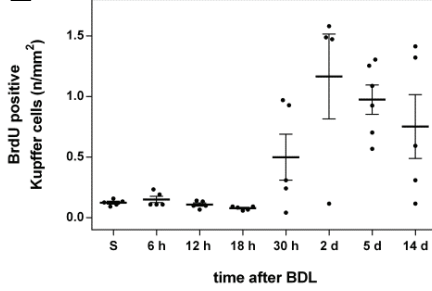
C



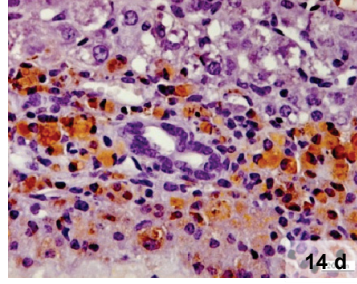
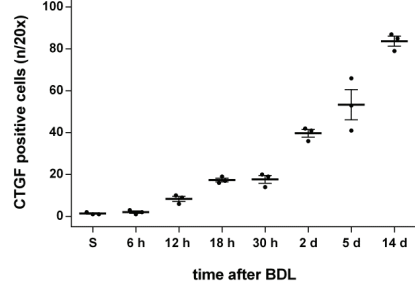
D



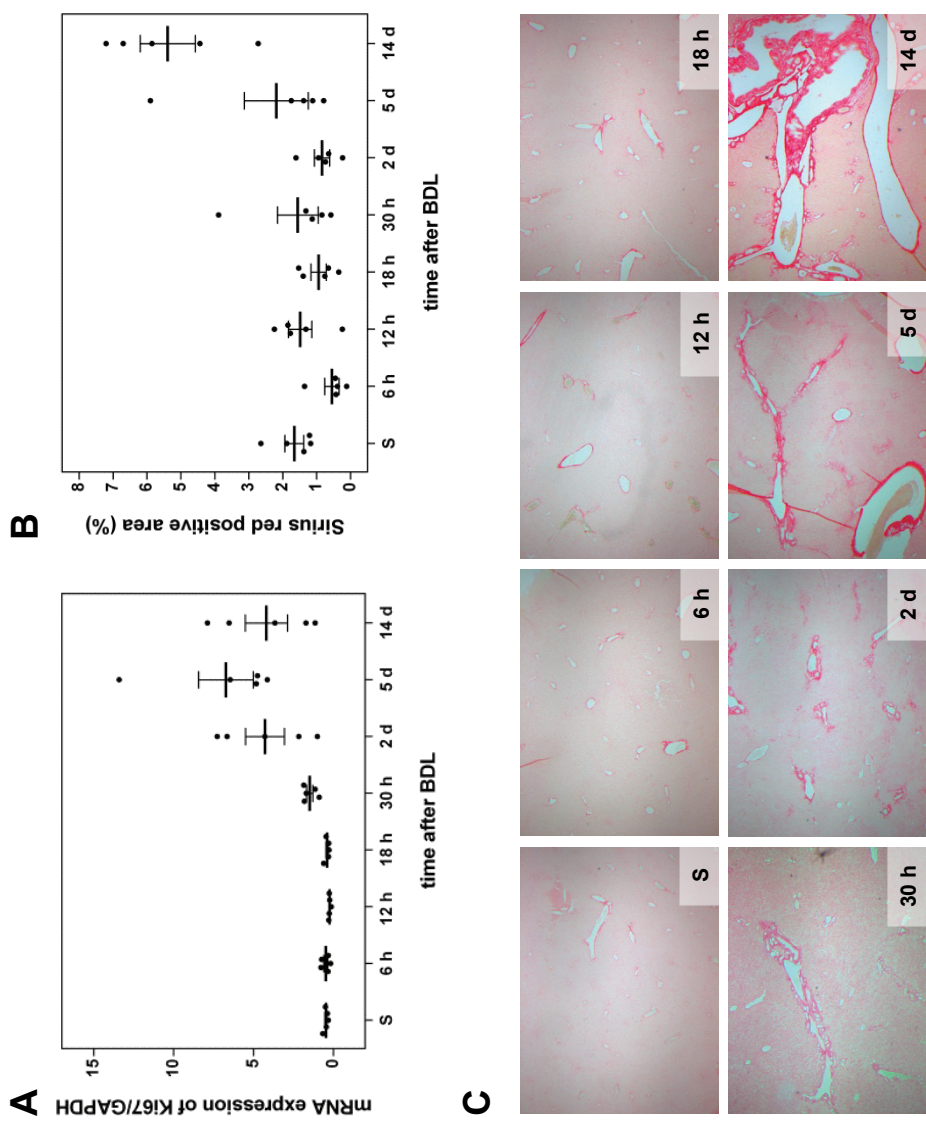
E



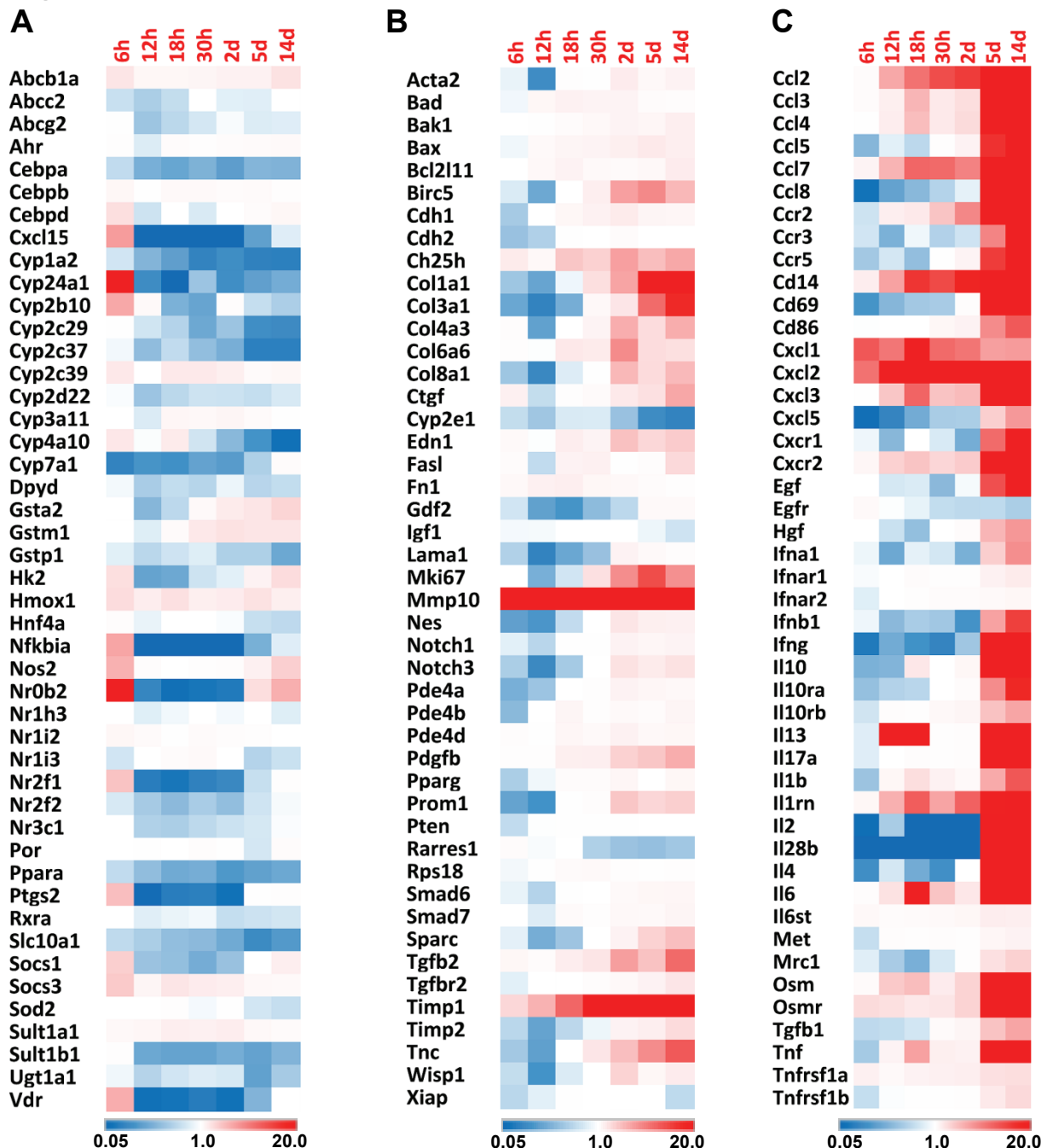
F

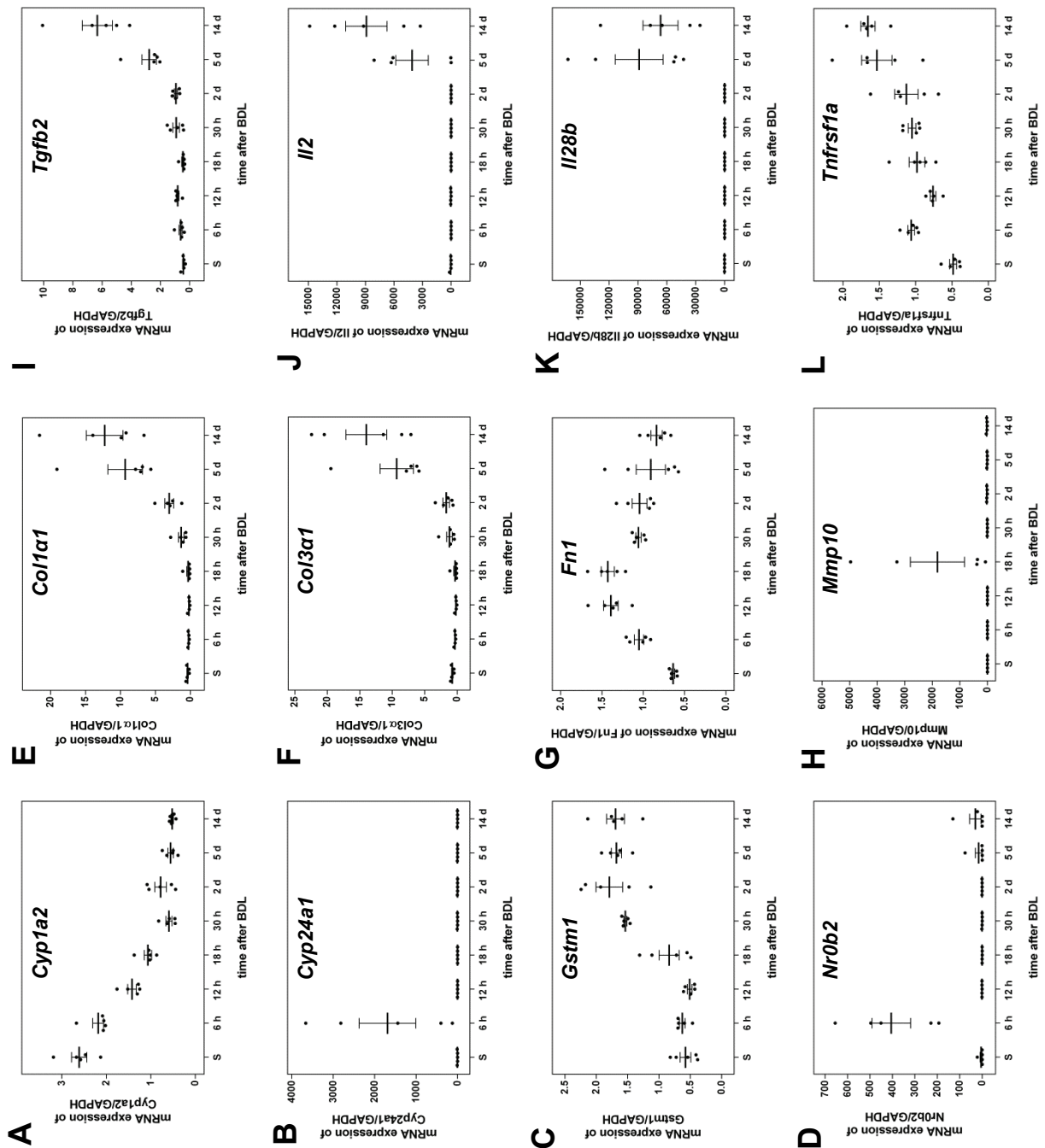


**Figure 4**

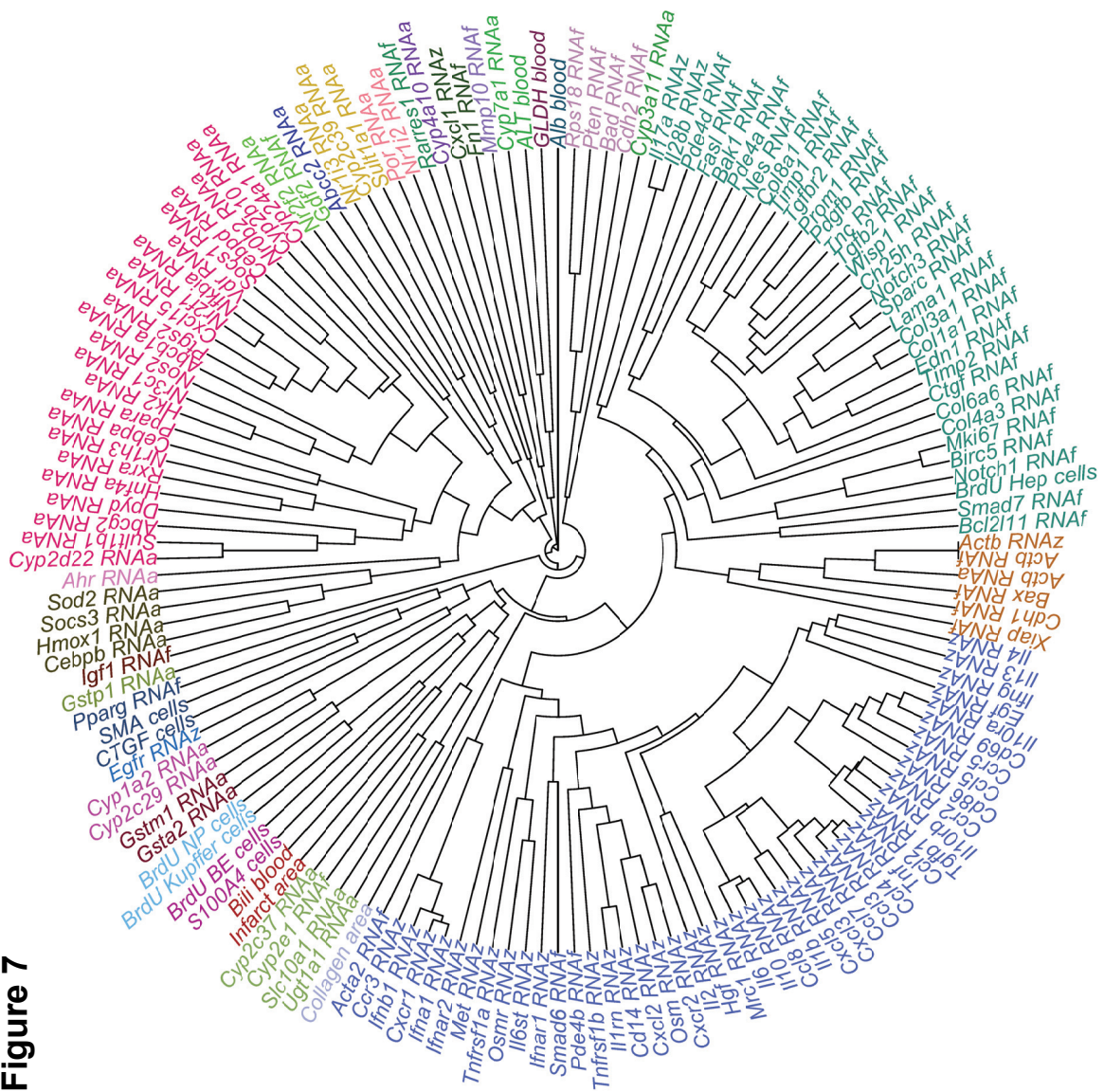


**Figure 5**

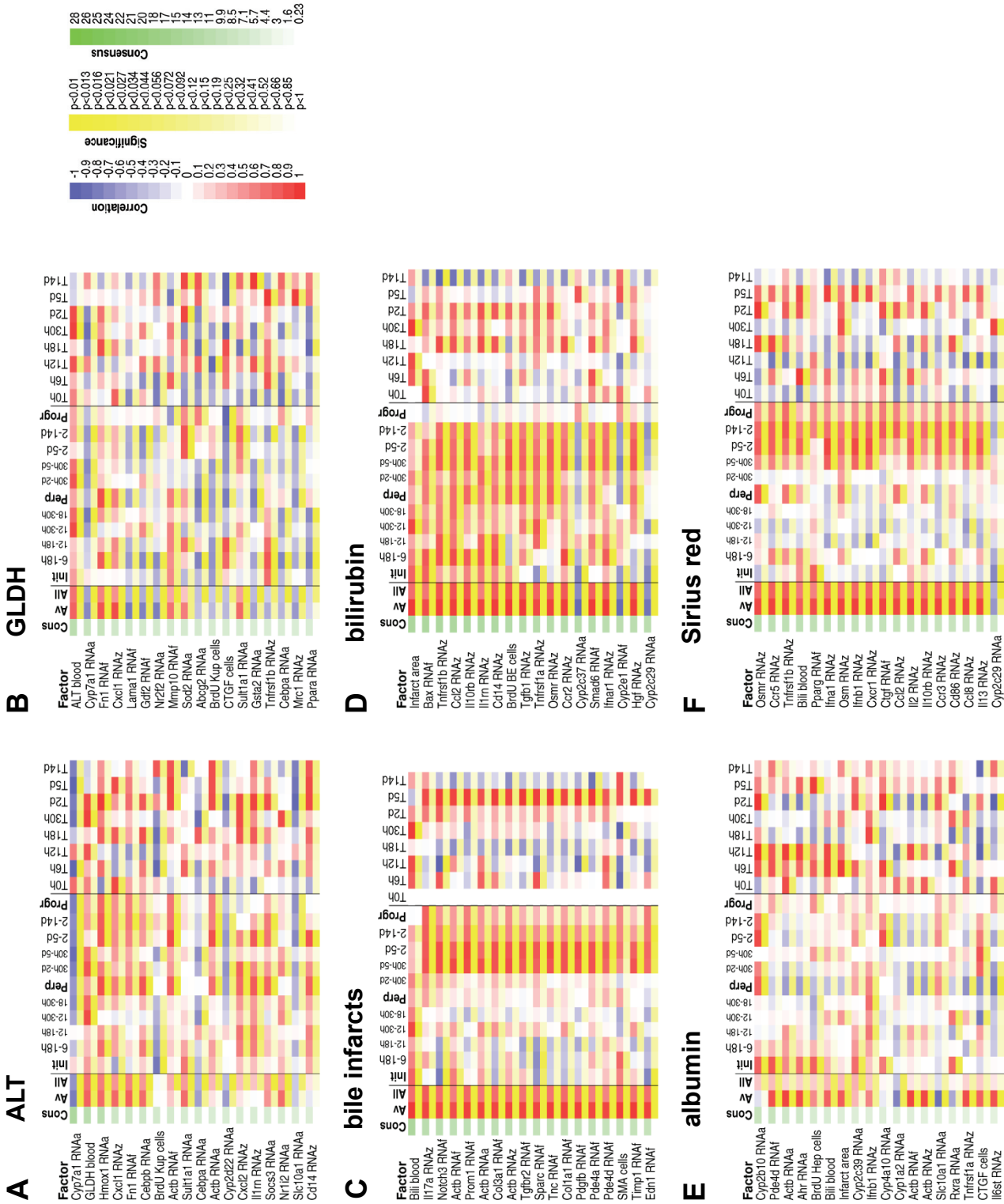


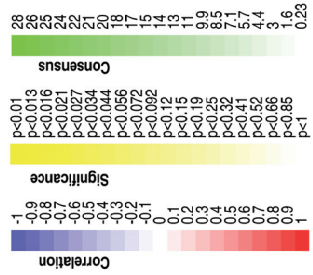
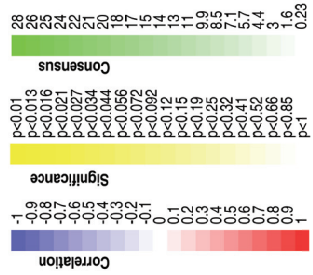
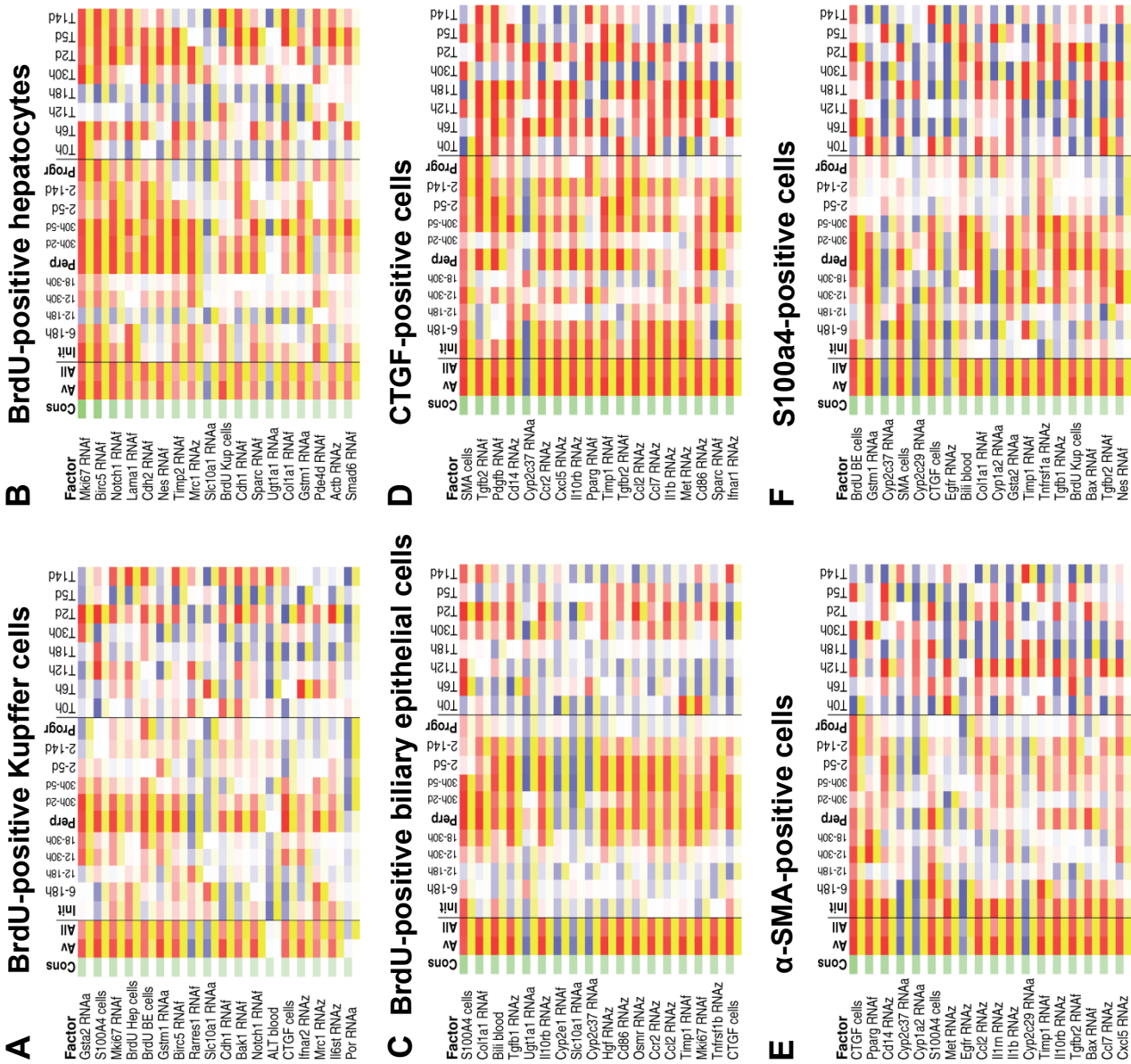
**Figure 6**

**Figure 7**



**Figure 8**



**Figure 9**

**Figure 10**

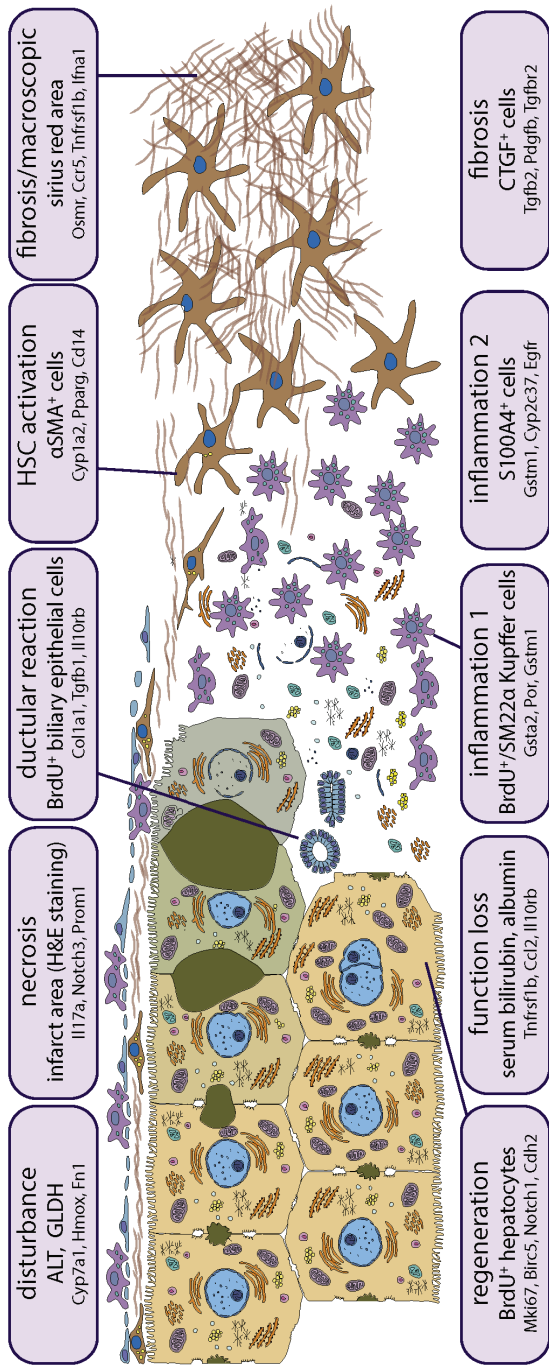
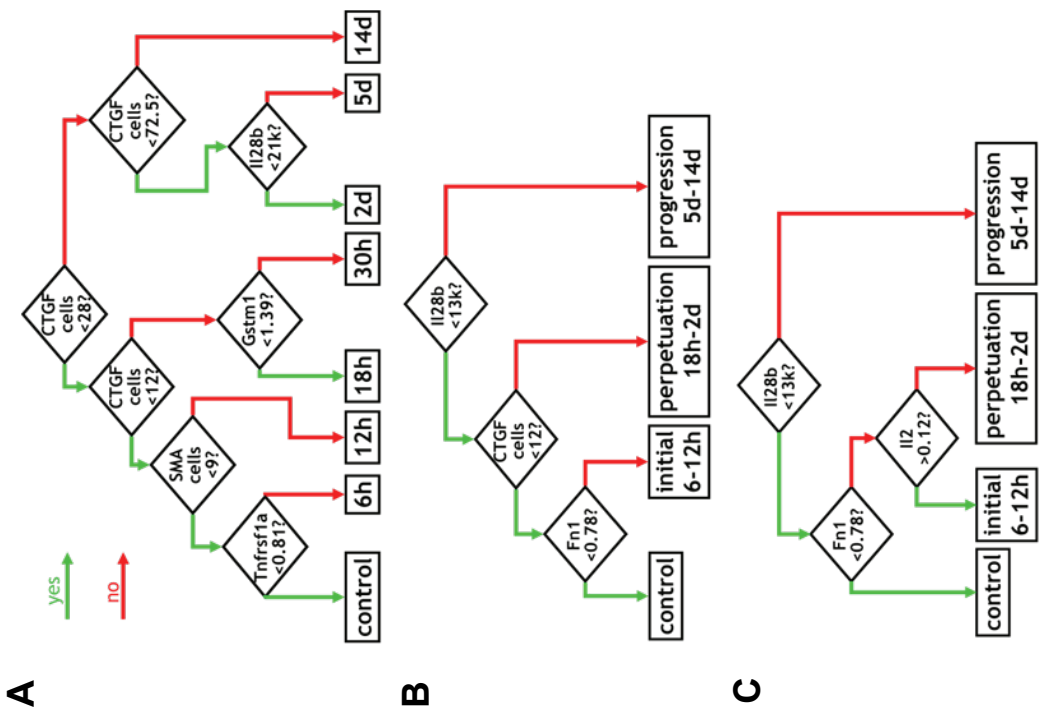


**Figure 11**



Supplement 1

[Click here to download Supplementary Material: Supplement1.pdf](#)

Supplement 2

[Click here to download Supplementary Material: Supplement2.pdf](#)

Supplement 3

[Click here to download Supplementary Material: Supplement3.pdf](#)

Supplement 4

[Click here to download Supplementary Material: Supplement4.pdf](#)